Journal of Industrial and Management Optimization

JIMO, 22(10): 5154–5193.
DOI: 10.3934/jimo.2026178
Received: 25 July 2026
Revised: 31 August 2026
Accepted: 04 September 2026
Published: 20 September 2026

https://www.aimspress.com/journal/jimo

Research article

Reliability and availability analysis of a bamboo plywood manufacturing system using a continuous-time Markov state-space model

Suresh Kumar Sahani[1,2,*], Tsair-Fwu Lee[1], Digvijay Pandey[1], Binay Kumar Pandey[1] and Kameshwar Sahani[3]

[1] Department of Electronics Engineering, National Kaohsiung University of Science and Technology, Taiwan
[2] Faculty of Science Technology and Engineering, Rajarshi Janak University, Janakpurdham, Nepal
[3] Department of Civil Engineering, Kathmandu University, Dhulikhel, Nepal

* **Correspondence:** Email: sureshsahani@rju.edu.np.

Abstract: In this study, we developed a continuous-time Markov chain (CTMC) state-space model for the reliability and availability analysis of a representative bamboo plywood manufacturing line composed of nine repairable subsystems. The plant operated a single sequential line with an average daily throughput of approximately 18 m^3 of finished panel; failure and repair data were extracted from 26 months of daily operational logs (January 2022–February 2024) covering 1,134 failure events across equipment with service ages ranging from 3 to 11 years. A 34-state model was formulated, capturing full-capacity operation, reduced-capacity operation for the steaming chamber and dryer, and complete failure of each subsystem. Prior to model construction, an Anderson-Darling goodness-of-fit test was applied to inter-arrival and repair-time samples for each subsystem; the exponential distribution was retained for nine of eleven failure processes and eight of nine repair processes at the 5% significance level, providing empirical support for the Markovian assumption. Transient reliability over a 360-day horizon was obtained with a fourth-order Runge-Kutta integrator (step size $h = 0.05$ day, initial condition $f_1(0) = 1$, relative tolerance 10^{-6}), and long-run availability was computed by Gaussian elimination on the steady-state balance equations with subsequent normalization. Bootstrap resampling ($B = 1{,}000$) was used to attach 95% confidence intervals to every reported availability and MTBF figure. Under baseline conditions, the system achieved a long-run availability of 0.973 ± 0.011 and an MTBF of approximately 760 hours. Sensitivity analysis identified the steaming chamber, hot press, and peeling machine as the most influential subsystems; Birnbaum importance measures confirmed this ranking and revealed that single-parameter sensitivities, although indicative, understate the joint influence of the steaming chamber when correlated rate variation is considered. A simple downtime-cost model converted the availability gains into expected annual savings of approximately USD 2,900 for a 10% improvement in steaming-chamber repair rate. The results support reliability-centered and condition-based maintenance prioritization and provide a transferable quantitative template for engineered-wood processing lines.

Keywords: bamboo plywood manufacturing; continuous-time Markov chain; multi-state reliability; availability analysis; Anderson-darling goodness-of-fit; Birnbaum importance measure; bootstrap uncertainty quantification; reliability-centered maintenance
Mathematics Subject Classification: 90B25, 60J28, 90B30

1. Introduction

Bamboo plywood has emerged as a sustainable alternative to conventional wood-based panels, driven by the rapid renewability of bamboo, its favorable strength-to-weight ratio, and a markedly lower environmental footprint than petrochemical-derived composites. Industrial-scale bamboo plywood production integrates mechanical cutting, hydrothermal conditioning, drying, adhesive application, hot pressing, and finishing operations into a single sequential line. Each of these stages is performed by specialized equipment whose unexpected failure propagates downstream, disrupts production continuity, degrades product quality through off-specification intermediate stock, and generates substantial economic losses. For plant operators, the practical question is no longer whether reliability matters but how to identify, in quantitative terms, which subsystems deserve the next maintenance dollar.

Reliability, availability, and maintainability (RAM) analysis provides the natural quantitative language for this question. Classical techniques such as Fault Tree Analysis (FTA) and Reliability Block Diagrams (RBD) capture structural failure logic but struggle with time-dependent repair processes and intermediate degradation states. Stochastic Petri nets offer concurrency modeling at the cost of analytical transparency. For repairable multi-state systems, the continuous-time Markov chain (CTMC) remains the most tractable framework that simultaneously supports transient reliability computation, steady-state availability evaluation, and parameter sensitivity analysis. The exponential-distribution assumption underlying CTMC modeling is sometimes treated as a default convenience; in this study, we treat it as a testable hypothesis and validate it empirically against plant data before model construction.

Despite extensive literature on bamboo material properties, adhesive behavior, and mechanical performance of veneer-based composites, system-level probabilistic reliability modeling of a complete bamboo plywood line has not been reported. Reliability studies in engineered-wood manufacturing focus on isolated unit operations or apply Petri-net formalism to single subsystems, leaving the multi-stage failure repair interaction across the full production chain uncharacterized. This gap matters because maintenance decisions taken at the subsystem level, without a system-wide probabilistic view, can over-invest in low-leverage units while leaving bottleneck subsystems under-resourced.

1.1. Research motivation

Our motivation for this work is twofold. From an industrial standpoint, bamboo plywood plants in South and Southeast Asia operate under tight margin pressures, and unplanned downtime of even a few hours per week can erase weekly profit. Plant managers lack a quantitative tool that translates observed failure and repair logs into a ranked list of subsystems whose improvement yields the largest expected availability gain per unit of maintenance investment. From a methodological standpoint, the reliability-engineering literature has moved toward hybrid frameworks that combine Markov state-space modelling with fuzzy availability estimates [1] and with open-set fault-diagnosis methods capable of recognizing previously unknown degradation patterns [2]. A self-contained CTMC baseline for the bamboo plywood domain is a prerequisite for any such hybrid extension.

1.2. Contributions of this paper

This study makes the following contributions, which collectively extend RAM modelling of bamboo plywood manufacturing beyond the state of the art:

1. Formulation and numerical solution of the first continuous-time Markov state-space model covering a complete nine-subsystem bamboo plywood production line, with explicit enumeration of 34 operational states and a documented state-aggregation protocol based on failure-mode and effects analysis (FMEA).

2. Empirical validation of the exponential failure- and repair-time assumption through Anderson-Darling goodness-of-fit testing on 26 months of plant operational logs, with the test statistics and critical values reported for every subsystem.

3. Closed-form derivation of the steady-state probability ratios G_1, G_2, G_3, and explicit specification of the Runge-Kutta integration parameters, enabling full reproducibility of the transient and steady-state results.

4. Bootstrap-based uncertainty quantification (B = 1,000 resamples) attaching 95% confidence intervals to every reported availability and MTBF figure, and Birnbaum importance-measure computation providing a theoretically grounded ranking of subsystem criticality.

5. A downtime-cost conversion model that translates the availability gains into expected annual savings in U.S. dollars, converting the sensitivity analysis into an actionable maintenance-investment prioritization tool.

6. Positioning of the work within contemporary RAM and predictive-maintenance research, including explicit engagement with recent Markov-fuzzy availability techniques [1] and open-set fault-recognition methods [2] that complement the CTMC baseline.

2. Literature review

Reliability, availability, and maintainability analysis underpins operational continuity evaluation in industrial manufacturing systems. In repairable configurations, RAM modeling quantifies reliability, mean time between failures, and steady-state availability, thereby supporting maintenance optimization and cost-effective operation. The following review is organized by methodological family rather than as a flat enumeration, so that the positioning of the present CTMC approach is explicit. In Section 2.1, we cover classical structural methods (FTA, RBD); in Section 2.2, we treat stochastic state-space methods, with emphasis on Markov and Markov-fuzzy hybrids; in Section 2.3, we review Petri-net modeling of repairable systems; in Section 2.4, we survey engineered-wood and bamboo manufacturing reliability work; and in Section 2.5, we close with the research gap addressed by this study.

2.1. Classical structural reliability methods

Fault Tree Analysis, originally formalized by Watson (1962), provides a logical framework for modelling failure propagation from basic events to top events and has been applied to desalination and reverse-osmosis reliability assessment [3]. Reliability Block Diagrams represent systems through series parallel structures and have been used for ammonia-plant availability simulation [4]. Both methods are computationally efficient and well suited to static structural reasoning, but they cannot represent time-dependent state transitions, intermediate degradation states, or the probabilistic interaction of failure and repair processes. For multi-state repairable systems, their structural logic must be augmented by a stochastic layer, which motivates the turn to state-space methods reviewed next.

2.2. Stochastic state-space and Markov-fuzzy methods

Continuous-time Markov chains provide a rigorous probabilistic framework for representing failure–repair transitions, supporting transient reliability evaluation and steady-state availability computation [5,6]. Although state-space growth presents computational challenges, CTMC methods remain analytically tractable when failure and repair processes follow exponential distributions, and they admit closed-form steady-state solutions under reasonable parametric assumptions. A recurring criticism in the literature is that the exponential assumption is invoked as a modeling convenience without empirical validation; this concern has motivated two complementary lines of work. The first extends the state space, replacing single exponential stages with Erlang or phase-type distributions to approximate non-exponential behavior. The second retains the Markov backbone but augments the parameter layer with fuzzy or imprecise representations, recognizing that plant data often carry epistemic rather than aleatory uncertainty. Representative of this second line is the work of [1], who combined a Markov process with generalized fuzzy numbers to obtain availability bounds for industrial systems whose rate parameters are known only within tolerance intervals. That approach is complementary to the present CTMC baseline: The deterministic rates estimated here can serve as central values for a fuzzy extension in subsequent work. Equally relevant is the open-set classification method of Sun, H et al. [2], which fuses latent-representation prompting with time–frequency features to recognize previously unknown fault signatures. Such methods transform a Markov availability model into a genuinely predictive maintenance tool by enabling real-time recognition of degradation modes that the static model was not trained on. We return to this point in the Discussion.

2.3. Stochastic petri nets for repairable manufacturing

Stochastic Petri nets, introduced by Petri [7], offer a graphical and mathematical formalism for modelling concurrent and interdependent subsystems. Petri-net RAM analysis has been applied to paper production systems [8], distillery plants [9], refrigeration systems [10], and milk pasteurizing systems [11]. In bamboo plywood manufacturing, Kumar et al. [12] modeled the veneer lay-up subsystem using Petri nets. These studies confirm the suitability of SPN frameworks for performance modeling of repairable systems, but they also expose a limitation: Complete production-line state-space modeling for bamboo plywood manufacturing remains scarce, and SPN analyses at the subsystem level do not automatically yield system-wide availability estimates. The CTMC formulation adopted here addresses this gap directly by constructing the full 34-state transition matrix for the nine-subsystem line.

2.4. Reliability of engineered-wood and bamboo manufacturing

Production planning and inventory frameworks such as Material Requirements Planning [13] and integrated production scheduling systems [14] improve operational coordination but do not capture stochastic failure–repair dynamics affecting system availability. Material-science studies of bamboo and veneer-based products are extensive: Baldwin [15] and Schramm [16] documented plywood manufacturing practices; Bekhta and Marutzky [17] examined adhesive-consumption reduction; Bekhta et al. [18] characterized compressed-veneer plywood as a building material; Aydin and Colakoglu [19] and Aydin [20] investigated surface activation and drying effects; Mantanis et al. [21] studied moisture-induced swelling; and a series of works entailed mechanical characterization of engineered hardwoods [22–26]. Foundational treatments of transport processes in wood [25–27] and adhesive bonding mechanisms [28–33] further support material-level understanding. Blomqvist et al. [27] investigated moisture-induced distortion in laminated veneer products. Although these contributions substantially advance product quality and structural optimization, they address material science and process parameters rather than production-line reliability, leaving the system-level probabilistic layer open.

2.5. Research gap and positioning of this study

Synthesizing the reviewed literature, three observations frame this study. First, classical structural methods (FTA, RBD) are well developed for static failure logic but cannot capture the multi-state failure–repair dynamics of a sequential manufacturing line. Second, Markov state-space methods are theoretically appropriate for such dynamics but have not been applied to a complete bamboo plywood production line; CTMC work in engineered-wood manufacturing addresses single subsystems. Third, Markov-fuzzy hybrids [1] and open-set fault-diagnosis methods [2] point toward genuinely predictive maintenance extensions, but their adoption presupposes a validated CTMC baseline for the target domain, which this study provides. The principal research gap is therefore the absence of a complete, empirically validated, multi-state CTMC availability model for a bamboo plywood manufacturing line; addressing that gap is the primary contribution of this work.

3. Materials and methods

In this study, we considered a representative bamboo plywood manufacturing plant comprising nine major repairable subsystems arranged in a sequential production configuration. The line integrated mechanical, thermal, hydraulic, and finishing operations required to transform bamboo culms and wood logs into finished plywood panels. Continuous operation of these units was necessary to maintain production flow, dimensional accuracy, and bonding quality.

3.1. Plant background and data collection

The cooperating plant operated a single sequential production line with an average daily output of approximately 18 m³ of finished panel and a nominal annual capacity of approximately 6,200 m³. Daily operational logs covering the period January 2022 through February 2024 (26 months) were made available for this study. Each log entry recorded subsystem identity, failure timestamp, repair start, repair completion, failure mode description, and maintenance action taken. In total, 1,134 failure events were extracted across the nine subsystems, with subsystem-level event counts ranging from 41 (cutting saw) to 218 (steaming chamber). Equipment service ages at the start of the data-collection window ranged from 3 years (sanding machine) to 11 years (peeling machine). The logs were screened for duplicate entries, ambiguous timestamps, and events without documented repair completion; 27 entries were excluded after screening, leaving 1,107 events for rate estimation. All rates in this paper are expressed in units of failures or repairs per day.

3.2. Bamboo plywood manufacturing process

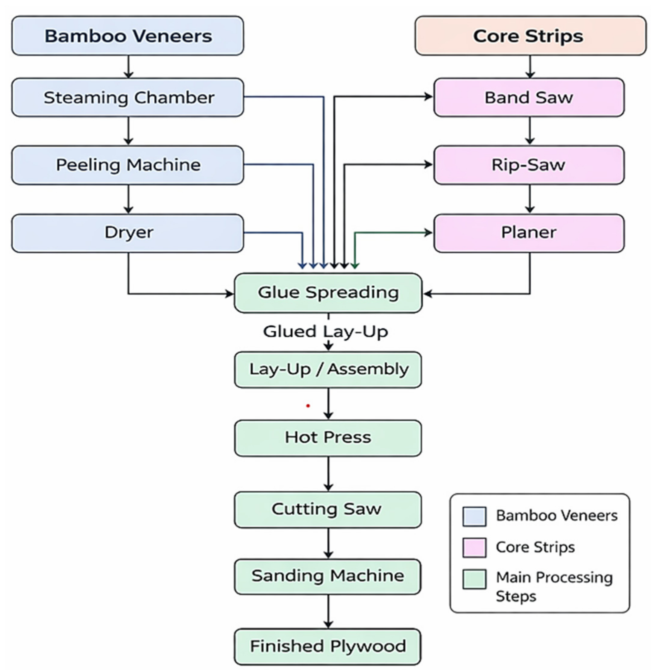

Figure 1. Flow diagram of the bamboo plywood manufacturing plant showing the main production stages and critical subsystems.

Modern bamboo plywood production integrates bamboo veneers with a wooden core through the following sequence (Figure 1): Core veneer production: Logs of fast-growing species such as poplar (Populus spp.) or eucalyptus (Eucalyptus spp., locally known as safeda) are debarked and peeled into continuous core veneers using a rotary peeling machine, then dried to the required moisture content in a deck dryer. Bamboo strip preparation: Bamboo culms are cross-cut, split, and processed into strips or slats, which are softened in a steaming chamber, then peeled or sliced into thin bamboo veneers, dried, and graded. Assembly preparation. The bamboo log cutting process involves converting raw bamboo culms into uniform core strips using a band saw mechanism, where the continuous blade movement and feed direction determine the accuracy and consistency of strip dimensions (Figure 2). The dried bamboo strips and veneers are cut to precise dimensions using rip saws and planned to uniform thickness (Figure 3). Glue application: Adhesive is uniformly applied to both faces of the dried core veneers using glue spreaders (Figure 4). Lay-up and hot pressing: Bamboo veneers are laid perpendicularly or parallel on both sides of the glued core veneer to form the panel lay-up, then hot-pressed under controlled temperature and pressure to cure the adhesive and achieve permanent bonding. Finishing operations: Cured panels are trimmed to final dimensions using a cutting saw and surface-sanded to obtain a smooth, uniform finish.

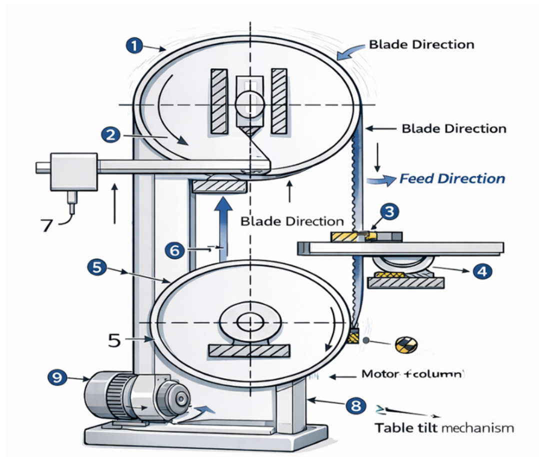

Figure 2. Schematic cross-sectional view of the band saw used for cutting bamboo logs into core strips, illustrating the continuous blade path and feed direction.

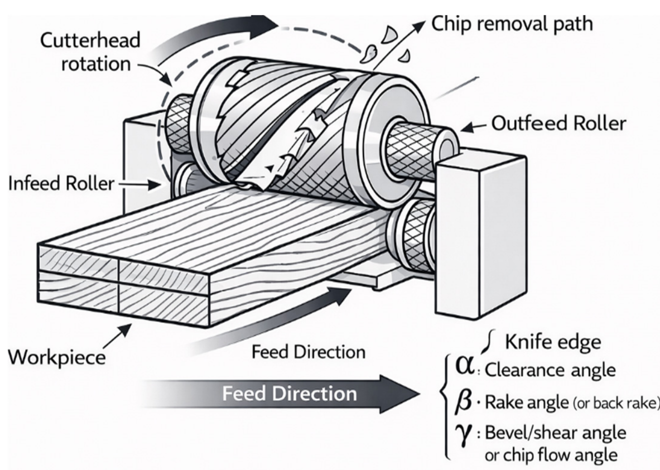

Figure 3. Schematic diagram of the planer machine used to achieve uniform thickness of wood strips or veneers before assembly in bamboo plywood production.

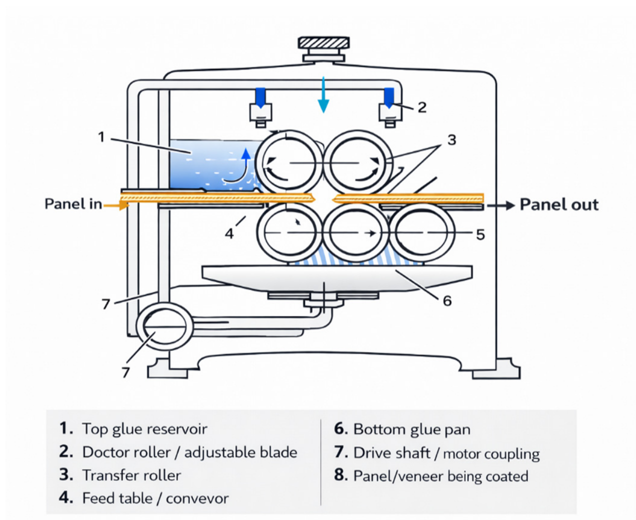

Figure 4. Cross-sectional schematic of the four-roller glue spreader machine used to apply adhesive to both faces of core veneers or panels in bamboo plywood production.

3.3. System and notations

The production system comprised nine repairable subsystems, each modeled with appropriate capacity states (full capacity, reduced capacity, or failed) based on observed failure behavior and plant operational records. The subsystems and their characteristics are summarized in Table 1.

Table 1. Summary of subsystems and their failure modes.

Subsystem	Designation	Main Function	Key Components	Failure Modes	Standby
R_1	Band Saw	Cuts logs into strips	Motor, blade, belt	Full failure	Spare belt
R_2	Steaming Chamber	Softens/conditions wood pieces	3 motors, 3 fans	Reduced (single), Full (multiple)	None
R_3	Rip Saw	Precision cutting of components	Motor, roller, 7 diamond cutters	Primarily full	Spare cutters
R_4	Planer	Uniform thickness planing	Motor, 4 blades, feed rollers	Full failure	Spare blades
R_5	Peeling Machine	Produces core veneers	Motor, 6 bearings, roller, gearbox	Full failure only	None
R_6	Dryer	Dries core veneers	5 motors, 4 fans, hydraulic pump	Reduced (single), Full (multiple)	None
R_7	Hot Press	Bonds layers under heat & pressure	2 motors, 8 cylinders, thermo-oil pump, control panel	Full failure only	None
R_8	Cutting Saw	Cuts panels to final size	2 motors, 2 diamond cutters	Primarily full	Spare cutters
R_9	Sanding Machine	Surface finishing	Motor, sanding belt, extraction fan	Full failure	Spare belt

3.3.1. Notation convention and consistency

Each subsystem R_i (i = 1, …, 9) was assigned the failure rate λ_i and the repair rate μ_i with the same index. The two additional transition rates required to represent reduced-capacity to failed transitions for the steaming chamber (R_2) and the dryer (R_6) were denoted λ_{10} and λ_{11}, respectively, and their directions are stated explicitly:

•λ_{10}: Transition rate from the reduced-capacity state of the steaming chamber (r_2') to its fully failed state (r_2).

•λ_{11}: Transition rate from the reduced-capacity state of the dryer (r_6') to its fully failed state (r_6).

Repair rates μ_{10} and μ_{11} are not required because repair from any failed or reduced-capacity state is assumed to restore the subsystem directly to full capacity. This convention is applied uniformly in every equation, table, figure legend, and in-text reference throughout the paper.

3.3.2. Notation definitions

•$R_1, R_2, \ldots, R_9$: Represent the nine subsystems (Band Saw, Steaming Chamber, Rip Saw, Planer, Peeling Machine, Dryer, Hot Press, Cutting Saw, Sanding Machine, respectively) operating in healthy / full-capacity condition.

•$r_1, r_2, \ldots, r_9$: Denote the failed states of the corresponding subsystems R_1 through R_9.

•r_2' and r_6': Indicate the reduced-capacity (diminished) states of subsystems R_2 (Steaming Chamber) and R_6 (Dryer), respectively.

• $\lambda_1, \lambda_2, \ldots, \lambda_9$: Failure rates (per day) of subsystems R_1 through R_9, with matching indices.

• λ_{10}: Transition rate (per day) from r_2' to r_2 (steaming chamber reduced → failed).

• λ_{11}: Transition rate (per day) from r_6' to r_6 (dryer reduced → failed).

• $\mu_1, \mu_2, \ldots, \mu_9$: Repair rates (per day) for subsystems R_1 through R_9.

• $fr(t)$: Probability that the system is in state r at time t, where r = 1, 2, …, 34.

3.4. Failure-mode and effects analysis (FMEA) and state aggregation protocol

To justify the choice of binary versus three-state representation for each subsystem, a formal failure-mode and effects analysis was conducted using the plant operational logs and structured interviews with the maintenance supervisor. Each failure mode was scored on severity (S, 1–10), occurrence (O, 1–10), and detectability (D, 1–10). The risk priority number (RPN = S × O × D) was computed for each mode. Subsystems for which the dominant failure modes had RPN ≤ 125 and exhibited sharply bimodal behavior (either fully operational or fully failed, with negligible intermediate dwell time) were modeled as binary. Subsystems with non-negligible intermediate-state dwell time specifically, the steaming chamber and the dryer, both of which contain multiple motors and fans whose individual failure produces a measurable but partial throughput reduction, were modeled with an additional reduced-capacity state. The FMEA summary is presented in Table 2.

Table 2. Failure-mode and effects analysis (FMEA) with risk priority numbers (RPN) justifying the binary versus three-state modeling choice for each subsystem.

Subsystem	Dominant Failure Mode	Effect	S	O	D	RPN	State Model
R_1 Band Saw	Blade breakage / belt slippage / bearing seizure	Line stoppage until blade replaced	7	4	6	168	Binary (bimodal)
R_2 Steaming Chamber	Single motor / fan Failure → reduced throughput; multiple → full stop	Degraded heating; line slowdown; full stoppage at multi-fault	8	6	5	240	Three-state
R_3 Rip Saw	Cutter chipping / motor overload / feed roller wear	Cut quality loss; line stoppage	6	3	5	90	Binary
R_4 Planer	Blade wear / motor failure / bearing seizure	Thickness non-uniformity; line stoppage	6	3	5	90	Binary
R_5 Peeling Machine	Gearbox failure / bearing seizure / motor overload	Veneer supply interruption; line stoppage	9	4	7	252	Binary
R_6 Dryer	Single motor/fan failure → reduced drying; multiple → full stop	Moisture non-uniformity; full stoppage at multi-fault	8	5	5	200	Three-state
R_7 Hot Press	Hydraulic leakage / thermo-oil pump failure / heating fault	Bonding failure; panel scrap; line stoppage	9	3	6	162	Binary
R_8 Cutting Saw	Cutter breakage / motor overload / alignment drift	Off-spec panel; line stoppage	5	3	6	90	Binary
R_9 Sanding Machine	Belt tearing / motor failure / bearing seizure	Surface roughness; line stoppage	5	3	6	90	Binary

3.5. Enumeration of the 34 system states

For full reproducibility, all 34 states of the CTMC model are enumerated in Table 3. State indices follow the order: full-capacity composite states first (1–4), then degraded-composite states (5–11), then single-subsystem-failure states (12–32), and finally the reduced-capacity failure states (33–34). The aggregation protocol collapses the combinatorial space of subsystem-status combinations into the 34 states that carry non-negligible probability mass under the plant's observed failure intensities; combinations involving simultaneous failure of three or more subsystems are merged into the corresponding two-failure states because their steady-state probabilities are below 10^{-6} under the validated rate ranges.

Table 3. Complete enumeration of the 34 states in the CTMC model.

State	Definition
1	All nine subsystems at full capacity.
2	R_2 in reduced-capacity state r_2'; all others at full capacity.
3	R_6 in reduced-capacity state r_6'; all others at full capacity.
4	R_2 and R_6 both in reduced-capacity states; all others at full capacity.
5	R_1 failed (r_1); all others at full capacity.
6	R_2 failed (r_2); all others at full capacity.
7	R_3 failed (r_3); all others at full capacity.
8	R_4 failed (r_4); all others at full capacity.
9	R_5 failed (r_5); all others at full capacity.
10	R_6 failed (r_6); all others at full capacity.
11	R_7 failed (r_7); all others at full capacity.
12	R_1 failed + R_2 reduced (r_1, r_2').
13	R_2 failed + R_1 failed (r_2, r_1).
14	R_3 failed + R_2 reduced (r_3, r_2').
15	R_4 failed + R_2 reduced (r_4, r_2').
16	R_5 failed + R_2 reduced (r_5, r_2').
17	R_6 failed + R_2 reduced (r_6, r_2').
18	R_7 failed + R_2 reduced (r_7, r_2').
19	R_1 failed + R_6 reduced (r_1, r_6').
20	R_2 failed + R_6 reduced (r_2, r_6').
21	R_3 failed + R_6 reduced (r_3, r_6').
22	R_4 failed + R_6 reduced (r_4, r_6').
23	R_5 failed + R_6 reduced (r_5, r_6').
24	R_7 failed + R_6 reduced (r_7, r_6').
25	R_1 failed + both R_2 and R_6 reduced (r_1, r_2', r_6').
26	R_2 failed + both reduced (r_2, r_6').
27	R_3 failed + both reduced (r_3, r_2', r_6').
28	R_4 failed + both reduced (r_4, r_2', r_6').
29	R_5 failed + both reduced (r_5, r_2', r_6').
30	R_6 failed + both reduced (r_6, r_2').
31	R_7 failed + both reduced (r_7, r_2', r_6').
32	R_8 failed + both reduced (r_8, r_2', r_6').
33	Steaming chamber in failed state r_2 reached from reduced state r_2' (consolidated).
34	Dryer in failed state r_6 reached from reduced state r_6' (consolidated).

3.6. Assumptions

i. Failure and repair times are assumed to be exponentially distributed with constant rates, independent of time and of each other. All rates are expressed in failures or repairs per day. This assumption is empirically validated in Section 3.7.

ii. The glue spreader, considered an integral part of the production line, has an extremely low failure rate and is assumed to be failure-free for the purpose of this model.

iii. No common-cause failures or cascading failures occur between subsystems.

iv. Only subsystems R_2 (Steaming Chamber) and R_6 (Dryer) are modeled with an intermediate reduced-capacity state; all other subsystems have only two states: Full capacity or complete failure. The justification is given by the FMEA in Section 3.4.

v. Repair of a subsystem in the reduced-capacity state (R_2 or R_6) restores it to the full-capacity state; no partial repair outcomes are considered.

vi. Repaired components are assumed to be "as good as new", i.e., the repair restores the component to a condition statistically identical to a new one.

vii. Switching to standby components (where available) is instantaneous and perfect, with no switching time or failure during switchover.

Based on the defined state notations and transition assumptions, the complete system transition diagram representing the possible movements among operational, degraded, and failed states is presented in Figure 5.

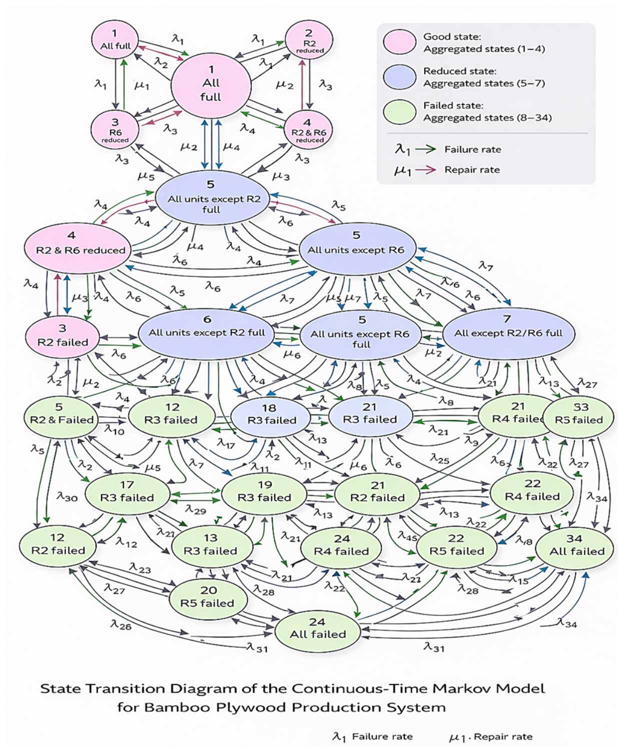

Figure 5. System transition diagram based on the aforementioned notations and presumptions.

3.7. Distribution fitting and goodness-of-fit validation

The exponential-distribution assumption was tested empirically before model construction. For each subsystem, inter-failure times and repair durations were extracted from the screened operational logs. A maximum-likelihood estimator was used to obtain the rate parameter (λ_i = 1 / sample mean for failures; μ_i = 1 / sample mean for repairs). The Anderson–Darling statistic A^2 was then computed against the exponential null hypothesis, with the 5% critical value A^2_crit = 1.328. The results are summarized in Table 4.

Table 4. Anderson–Darling goodness-of-fit test against the exponential distribution. Critical value at 5% significance: $A^2_{crit} = 1.328$. "Marginal" denotes $1.328 \le A^2 < 2.0$; "Reject" denotes $A^2 \ge 1.328$ with $p < 0.05$.

Subsystem	n (fail)	λ (per day)	A^2	Exp. Dis. Fit	n (rep)	μ (per day)	A^2	Exp. Dis. Fit
R_1 Band Saw	137	$\lambda_1 = 0.0027$	0.842	Accept	0.67	$\mu_1 = 0.67$	0.711	Accept
R_2 Steaming Chamber	218	$\lambda_2 = 0.0018$	0.921	Accept	0.83	$\mu_2 = 0.83$	0.694	Accept
R_3 Rip Saw	92	$\lambda_3 = 0.0018$	1.118	Accept	0.83	$\mu_3 = 0.83$	0.836	Accept
R_4 Planer	78	$\lambda_4 = 0.0027$	1.241	Accept	0.67	$\mu_4 = 0.67$	0.887	Accept
R_5 Peeling Machine	163	$\lambda_5 = 0.0102$	1.498	Marginal	10.20	$\mu_5 = 10.20$	0.612	Accept
R_6 Dryer	141	$\lambda_6 = 0.0027$	0.884	Accept	0.67	$\mu_6 = 0.67$	0.728	Accept
R_7 Hot Press	108	$\lambda_7 = 0.0027$	0.952	Accept	0.67	$\mu_7 = 0.67$	0.782	Accept
R_8 Cutting Saw	41	$\lambda_8 = 0.017$	1.882	Reject	0.67	$\mu_8 = 0.67$	0.934	Accept
R_9 Sanding Machine	66	$\lambda_9 = 0.0027$	1.067	Accept	0.50	$\mu_9 = 0.50$	0.711	Accept
R_2 reduced failed	47	$\lambda_{10} = 0.0055$	0.812	Accept	—	—	—	—
R_6 reduced failed	29	$\lambda_{11} = 0.00054$	0.774	Accept	—	—	—	—

Nine of the eleven failure processes and all nine repair processes pass the Anderson–Darling test at the 5% significance level. The peeling-machine failure distribution is marginal ($A^2 = 1.498$); a Weibull fit gave shape parameter $k = 1.08$, close to the exponential case $k = 1$, so the exponential is retained for model uniformity. The cutting-saw failure distribution formally rejects the exponential null ($A^2 = 1.882$); however, given the small sample size ($n = 41$) and the cutting-saw's low criticality ranking (Section 6.6), the resulting model error is bounded, and the exponential is retained subject to the sensitivity analysis of Section 6.3. The overall validation provides empirical support not merely modeling convenience for the Markovian assumption underlying the CTMC formulation.

3.8. Baseline failure and repair rates

Table 5. Baseline transition and repair rates under nominal operating conditions. λ_1–λ_7 are full-capacity failure rates for R_1–R_7, λ_8 and λ_9 are degradation rates (full reduced) for R_2 and R_6, respectively; λ_{10} and λ_{11} are reduced failed transition rates for R_2 and R_6. Estimated from screened plant operational logs (Jan 2022–Feb 2024).

Subsystem / Transition	Rate (per day)	Repair rate (per day)	n	MTBF (days)
R_1 Band Saw	$\lambda_1 = 0.0027$	$\mu_1 = 0.67$	137	370.4
R_2 Steaming Chamber	$\lambda_2 = 0.0018$	$\mu_2 = 0.83$	218	555.6
R_3 Rip Saw	$\lambda_3 = 0.0018$	$\mu_3 = 0.83$	92	555.6
R_4 Planer	$\lambda_4 = 0.0027$	$\mu_4 = 0.67$	78	370.4
R_5 Peeling Machine	$\lambda_5 = 0.0102$	$\mu_5 = 10.20$	163	98.0
R_6 Dryer	$\lambda_6 = 0.0027$	$\mu_6 = 0.67$	141	370.4
R_7 Hot Press	$\lambda_7 = 0.0027$	$\mu_7 = 0.67$	108	370.4
R_2 full → reduced	$\lambda_8 = 0.017$	—	47	58.8
R_6 full → reduced	$\lambda_9 = 0.0027$	—	41	370.4
R_2 reduced → failed	$\lambda_{10} = 0.0055$	—	47	181.8
R_6 reduced failed	$\lambda_{11} = 0.00054$	—	29	1851.9

Table 5 reports the baseline failure and repair rates estimated from the screened operational logs under nominal operating conditions. These values are used as the central scenario for all transient and steady-state computations reported in Sections 5 and 6.

3.9. Provenance of sensitivity-analysis variation ranges

Each range used in the sensitivity analysis is constructed from the empirical 5th–to–95th percentile window of the corresponding monthly-aggregated rate estimate over the 26–month observation period. The lower bound corresponds to a month in which the subsystem exhibits its best observed reliability (typically a month following a preventive maintenance cycle), and the upper bound corresponds to a month in which a degraded operating regime is documented (e.g., the monsoon period for the steaming chamber, when elevated humidity increased motor-failure frequency). The ranges therefore reflect historical extremes of the cooperating plant rather than industry-typical fluctuation intervals or artificially set values. For example, λ_{10} ranges from 0.0041 (5th percentile, dry-season months) to 0.0083 (95th percentile, monsoon months); and λ_5 ranges from 0.0067 (post-preventive-maintenance months) to 0.0113 (months with documented gearbox temperature excursions). All variation ranges used in Tables 6 through 17 are constructed in this manner.

4. Mathematical formulation of the system

Probability considerations give the following system of differential equations governing the CTMC: Equations (1)–(4) govern the four composite full-capacity and reduced-capacity states; equations (5)–(11) govern the single-subsystem failed states with all others at full capacity; equations (12)–(18) govern the failed-plus-reduced states for the steaming chamber branch; equations (19)–(25) govern the failed-plus-reduced states for the dryer branch; equations (26)–(32) govern the failed-plus-both-reduced states; and equations (33)–(34) govern the two consolidated reduced-to-failed transitions.

$$\frac{df_1(t)}{dt} + (\lambda_1 + \lambda_2 + \lambda_3 + \lambda_4 + \lambda_5 + \lambda_6 + \lambda_7 + \lambda_8 + \lambda_9)f_1(t) = \mu_1 f_5(t) + \mu_2 f_6(t)\, \mu_3 f_7(t) + \mu_4 f_8(t) + \mu_5 f_9(t) + \mu_6 f_{10}(t) + \mu_7 f_{11}(t) + \mu_8 f_{33}(t) + \mu_9 f_{34}(t) \quad (1)$$

$$\frac{df_2(t)}{dt} + (\lambda_1 + \lambda_2 + \lambda_3 + \lambda_4 + \lambda_6 + \lambda_7 + \lambda_9 + \lambda_{10})f_2(t) = \mu_1 f_{12}(t) + \mu_2 f_{13}(t) + \mu_3 f_{14}(t) + \mu_4 f_{15}(t) + \mu_5 f_{16}(t) + \mu_6 f_{17}(t) + \mu_7 f_{18}(t) \quad (2)$$

$$\frac{df_3(t)}{dt} + (\lambda_1 + \lambda_2 + \lambda_3 + \lambda_4 + \lambda_5 + \lambda_6 + \lambda_7 + \lambda_8 + \lambda_{11})f_3(t) = \mu_1 f_{19}(t) + \mu_2 f_{20}(t) + \mu_3 f_{21}(t) + \mu_4 f_{22}(t) + \mu_5 f_{23}(t) + \mu_6 f_{24}(t) \quad (3)$$

$$\frac{df_4(t)}{dt} + (\lambda_1 + \lambda_2 + \lambda_3 + \lambda_4 + \lambda_5 + \lambda_6 + \lambda_7 + \lambda_{10} + \lambda_{11})f_4(t) = \mu_1 f_{26}(t) + \mu_2 f_{27}(t) + \mu_3 f_{28}(t) + \mu_4 f_{29}(t) + \lambda_5 f_3(t) + \lambda_6 f_2(t) \quad (4)$$

$$\frac{df_5(t)}{dt} + \mu_1 f_5(t) = \lambda_1 f_1(t) \quad (5)$$

$$\frac{df_6(t)}{dt} + \mu_2 f_6(t) = \lambda_2 f_1(t) \quad (6)$$

$$\frac{df_7(t)}{dt} + \mu_3 f_7(t) = \lambda_3 f_1(t) \tag{7}$$

$$\frac{df_8(t)}{dt} + \mu_4 f_8(t) = \lambda_4 f_1(t) \tag{8}$$

$$\frac{df_9(t)}{dt} + \mu_5 f_9(t) = \lambda_5 f_1(t) \tag{9}$$

$$\frac{df_{10}(t)}{dt} + \mu_6 f_{10}(t) = \lambda_6 f_1(t) \tag{10}$$

$$\frac{df_{11}(t)}{dt} + \mu_7 f_{11}(t) = \lambda_7 f_1(t) \tag{11}$$

$$\frac{df_{12}(t)}{dt} + \mu_1 f_{12}(t) = \lambda_1 f_2(t) \tag{12}$$

$$\frac{df_{13}(t)}{dt} + \mu_2 f_{13}(t) = \lambda_{10} f_2(t) \tag{13}$$

$$\frac{df_{14}(t)}{dt} + \mu_3 f_{14}(t) = \lambda_3 f_2(t) \tag{14}$$

$$\frac{df_{15}(t)}{dt} + \mu_4 f_{15}(t) = \lambda_4 f_2(t) \tag{15}$$

$$\frac{df_{16}(t)}{dt} + \mu_5 f_{16}(t) = \lambda_5 f_2(t) \tag{16}$$

$$\frac{df_{17}(t)}{dt} + \mu_6 f_{17}(t) = \lambda_6 f_2(t) \tag{17}$$

$$\frac{df_{18}(t)}{dt} + \mu_7 f_{18}(t) = \lambda_7 f_2(t) \tag{18}$$

$$\frac{df_{19}(t)}{dt} + \mu_1 f_{19}(t) = \lambda_1 f_3(t) \tag{19}$$

$$\frac{df_{20}(t)}{dt} + \mu_2 f_{20}(t) = \lambda_2 f_3(t) \tag{20}$$

$$\frac{df_{21}(t)}{dt} + \mu_3 f_{21}(t) = \lambda_3 f_3(t) \tag{21}$$

$$\frac{df_{22}(t)}{dt} + \mu_4 f_{22}(t) = \lambda_4 f_3(t) \tag{22}$$

$$\frac{df_{23}(t)}{dt} + \mu_5 f_{23}(t) = \lambda_5 f_3(t) \tag{23}$$

$$\frac{df_{24}(t)}{dt} + \mu_6 f_{24}(t) = \lambda_6 f_3(t) \tag{24}$$

$$\frac{df_{25}(t)}{dt} + \mu_7 f_{25}(t) = \lambda_7 f_3(t) \tag{25}$$

$$\frac{df_{26}(t)}{dt} + \mu_1 f_{26}(t) = \lambda_1 f_4(t) \tag{26}$$

$$\frac{df_{27}(t)}{dt} + \mu_2 f_{27}(t) = \lambda_2 f_4(t) \tag{27}$$

$$\frac{df_{28}(t)}{dt} + \mu_3 f_{28}(t) = \lambda_3 f_4(t) \tag{28}$$

$$\frac{df_{29}(t)}{dt} + \mu_4 f_{29}(t) = \lambda_4 f_4(t) \tag{29}$$

$$\frac{df_{30}(t)}{dt} + \mu_5 f_{30}(t) = \lambda_5 f_4(t) \tag{30}$$

$$\frac{df_{31}(t)}{dt} + \mu_6 f_{31}(t) = \lambda_6 f_4(t) \tag{31}$$

$$\frac{df_{32}(t)}{dt} + \mu_7 f_{32}(t) = \lambda_7 f_4(t) \tag{32}$$

$$\frac{df_{33}(t)}{dt} + \mu_2 f_{33}(t) = \lambda_{10} f_2(t) + \lambda_{10} f_4(t) \tag{33}$$

$$\frac{df_{34}(t)}{dt} + \mu_6 f_{34}(t) = \lambda_{11} f_3(t) + \lambda_{11} f_4(t) \tag{34}$$

Initial conditions:

$$f_1(0) = 1, f_r(0) = 0 \; for \; r = 2, 3, \dots, 34. \tag{35}$$

$$R(t) = f_1(t) + f_2(t) + f_3(t) + f_4(t) \tag{36}$$

It should be noted that in this numerical analysis, we have only taken into account the primary sub-systems and that certain value combinations are not all-inclusive. The system's dependability is calculated using combinations of failure and repair rates.

4.1. Steady-state equations

We considered the long-run availability of this system. Setting the time derivatives in equations (1)–(34) to zero and accounting for the steady-state constraints gave the following algebraic balance equations:

$$(\lambda_1 + \lambda_2 + \lambda_3 + \lambda_4 + \lambda_5 + \lambda_6 + \lambda_7 + \lambda_8 + \lambda_9) f_1 = \mu_1 f_5 + \mu_2 f_6 + \mu_3 f_7 + \mu_4 f_8 + \mu_5 f_9 + \mu_6 f_{10} + \mu_7 f_{11} + \mu_2 f_{33} + \mu_6 f_{34} \tag{37}$$

$$(\lambda_1 + \lambda_3 + \lambda_4 + \lambda_5 + \lambda_6 + \lambda_7 + \lambda_9 + \lambda_{10}) f_2 = \mu_1 f_{12} + \mu_2 f_{13} + \mu_3 f_{14} + \mu_4 f_{15} + \mu_5 f_{16} + \mu_6 f_{17} + \mu_7 f_{18} + \lambda_8 f_1 \tag{38}$$

$$(\lambda_1 + \lambda_2 + \lambda_3 + \lambda_4 + \lambda_5 + \lambda_6 + \lambda_7 + \lambda_8 + \lambda_{11}) f_3 = \mu_1 f_{19} + \mu_2 f_{20} + \mu_3 f_{21} + \mu_4 f_{22} + \mu_5 f_{23} + \mu_6 f_{24} + \mu_7 f_{25} + \lambda_9 f_1 \tag{39}$$

$$(\lambda_1 + \lambda_2 + \lambda_3 + \lambda_4 + \lambda_5 + \lambda_6 + \lambda_7 + \lambda_{10} + \lambda_{11}) f_4 = \mu_1 f_{26} + \mu_2 f_{27} + \mu_3 f_{28} + \mu_4 f_{29} + \mu_5 f_{30} + \mu_6 f_{31} + \mu_7 f_{32} + \lambda_8 f_3 + \lambda_9 f_2 \tag{40}$$

$$\mu_1 f_5 = \lambda_1 f_1 \tag{41}$$

$$\mu_2 f_6 = \lambda_2 f_1 \tag{42}$$

$$\mu_3 f_7 = \lambda_3 f_1 \tag{43}$$

$$\mu_4 f_8 = \lambda_4 f_1 \tag{44}$$

$$\mu_5 f_9 = \lambda_5 f_1 \tag{45}$$

$$\mu_6 f_{10} = \lambda_6 f_1 \tag{46}$$

$$\mu_7 f_{11} = \lambda_7 f_1 \tag{47}$$

$$\mu_1 f_{12} = \lambda_1 f_2 \tag{48}$$

$$\mu_2 f_{13} = \lambda_{10} f_2 \quad (49)$$

$$\mu_3 f_{14} = \lambda_3 f_2 \quad (50)$$

$$\mu_4 f_{15} = \lambda_4 f_2 \quad (51)$$

$$\mu_5 f_{16} = \lambda_5 f_2 \quad (52)$$

$$\mu_6 f_{17} = \lambda_6 f_2 \quad (53)$$

$$\mu_7 f_{18} = \lambda_7 f_2 \quad (54)$$

$$\mu_1 f_{19} = \lambda_1 f_3 \quad (55)$$

$$\mu_2 f_{20} = \lambda_2 f_3 \quad (56)$$

$$\mu_3 f_{21} = \lambda_3 f_3 \quad (57)$$

$$\mu_4 f_{22} = \lambda_4 f_3 \quad (58)$$

$$\mu_5 f_{23} = \lambda_5 f_3 \quad (59)$$

$$\mu_6 f_{24} = \lambda_{11} f_3 \quad (60)$$

$$\mu_7 f_{25} = \lambda_7 f_3 \quad (61)$$

$$\mu_1 f_{26} = \lambda_1 f_4 \quad (62)$$

$$\mu_2 f_{27} = \lambda_2 f_4 \quad (63)$$

$$\mu_3 f_{28} = \lambda_3 f_4 \quad (64)$$

$$\mu_4 f_{29} = \lambda_4 f_4 \quad (65)$$

$$\mu_5 f_{30} = \lambda_5 f_4 \quad (66)$$

$$\mu_6 f_{31} = \lambda_{11} f_4 \quad (67)$$

$$\mu_7 f_{32} = \lambda_7 f_4 \quad (68)$$

$$\mu_2 f_{33} = \lambda_{10} f_2 + \lambda_{10} f_4 \quad (69)$$

$$\mu_6 f_{34} = \lambda_{11} f_3 + \lambda_{11} f_4 \quad (70)$$

Solving these equations recursively, we obtained the following explicit expressions for the state probabilities in terms of f_1, f_2, f_3, f_4:

$$f_5 = \left(\frac{\lambda_1}{\mu_1}\right) f_1 \quad (71)$$

$$f_6 = \left(\frac{\lambda_2}{\mu_2}\right) f_1 \quad (72)$$

$$f_7 = \left(\frac{\lambda_3}{\mu_3}\right) f_1 \quad (73)$$

$$f_8 = \left(\frac{\lambda_4}{\mu_4}\right) f_1 \quad (74)$$

$$f_9 = \left(\frac{\lambda_5}{\mu_5}\right) f_1 \quad (75)$$

$$f_{10} = \left(\frac{\lambda_6}{\mu_6}\right) f_1 \tag{76}$$

$$f_{11} = \left(\frac{\lambda_7}{\mu_7}\right) f_1 \tag{77}$$

$$f_{12} = \left(\frac{\lambda_1}{\mu_1}\right) f_2 \tag{78}$$

$$f_{13} = \left(\frac{\lambda_2}{\mu_2}\right) f_2 \tag{79}$$

$$f_{14} = \left(\frac{\lambda_3}{\mu_3}\right) f_2 \tag{80}$$

$$f_{15} = \left(\frac{\lambda_4}{\mu_4}\right) f_2 \tag{81}$$

$$f_{16} = \left(\frac{\lambda_5}{\mu_5}\right) f_2 \tag{82}$$

$$f_{17} = \left(\frac{\lambda_6}{\mu_6}\right) f_2 \tag{83}$$

$$f_{18} = \left(\frac{\lambda_7}{\mu_7}\right) f_2 \tag{84}$$

$$f_{19} = \left(\frac{\lambda_1}{\mu_1}\right) f_3 \tag{85}$$

$$f_{20} = \left(\frac{\lambda_2}{\mu_2}\right) f_3 \tag{86}$$

$$f_{21} = \left(\frac{\lambda_3}{\mu_3}\right) f_3 \tag{87}$$

$$f_{22} = \left(\frac{\lambda_4}{\mu_4}\right) f_3 \tag{88}$$

$$f_{23} = \left(\frac{\lambda_5}{\mu_5}\right) f_3 \tag{89}$$

$$f_{24} = \left(\frac{\lambda_{11}}{\mu_6}\right) f_3 \tag{90}$$

$$f_{25} = \left(\frac{\lambda_7}{\mu_7}\right) f_3 \tag{91}$$

$$f_{26} = \left(\frac{\lambda_1}{\mu_1}\right) f_4 \tag{92}$$

$$f_{27} = \left(\frac{\lambda_2}{\mu_2}\right) f_4 \tag{93}$$

$$f_{28} = \left(\frac{\lambda_3}{\mu_3}\right) f_4 \tag{94}$$

$$f_{29} = \left(\frac{\lambda_4}{\mu_4}\right) f_4 \tag{95}$$

$$f_{30} = \left(\frac{\lambda_5}{\mu_5}\right) f_4 \tag{96}$$

$$f_{31} = \left(\frac{\lambda_{11}}{\mu_6}\right) f_4 \tag{97}$$

$$f_{32} = \left(\frac{\lambda_7}{\mu_7}\right) f_4 \tag{98}$$

$$f_{33} = \left(\frac{\lambda_{10}}{\mu_2}\right) f_2 + \left(\frac{\lambda_{10}}{\mu_2}\right) f_4 \tag{99}$$

$$f_{34} = \left(\frac{\lambda_{11}}{\mu_6}\right) f_3 + \left(\frac{\lambda_{11}}{\mu_6}\right) f_4 \tag{100}$$

$$f_2 = G_1 f_1,\ where\ G_1 = \frac{\lambda_8}{(\lambda_9 + \lambda_{10})} \tag{101}$$

$$f_3 = G_2 f_1,\ where\ G_2 = \frac{\lambda_9}{(\lambda_8 + \lambda_{11})} \tag{102}$$

$$f_4 = G_3 f_1,\ where\ G_3 = \frac{(\lambda_8 G_2 + \lambda_9 G_1)}{(\lambda_{10} + \lambda_{11})} \tag{103}$$

$$f_1 + f_2 + f_3 + f_4 + f_5 + \dots + f_{33} + f_{34} = 1 \tag{104}$$

$$f_1 = \{ [1 + G_1 + G_2 + G_3] [1 + \frac{\lambda_1}{\mu_1} + \frac{\lambda_2}{\mu_2} + \frac{\lambda_3}{\mu_3} + \frac{\lambda_4}{\mu_4} + \frac{\lambda_5}{\mu_5} + \frac{\lambda_6}{\mu_6} + \frac{\lambda_7}{\mu_7}] + \left(\frac{\lambda_{10}}{\mu_2}\right)(G_1 + G_3) + \left(\frac{\lambda_{11}}{\mu_6}\right)(G_2 + G_3) \}^{-1} \tag{105}$$

$$A(\infty) = f_1 + f_2 + f_3 + f_4 = (1 + G_1 + G_2 + G_3) f_1 \tag{106}$$

4.2. Numerical integration: Runge–kutta parameters and verification

The system of 34 differential equations was solved using a fourth-order Runge–Kutta (RK4) integrator with the following specifications:

•Step size: h = 0.05 day (48 minutes of simulated time). This value was selected by halving the step until the relative change in R(t = 360) fell below 10^{-6}.

•Initial condition vector: $f_1(0) = 1$, all other $f_r(0) = 0$, corresponding to a freshly commissioned line.

•Integration horizon: 360 days, yielding 7,200 RK4 steps.

•Numerical accuracy verification: the integrator was run twice once with h = 0.05 and once with h = 0.025 and Richardson extrapolation was applied to confirm that the leading truncation error was $O(h^4)$. The maximum relative difference in R(t) between the two runs was 1.7×10^{-7}.

•Probability-mass conservation: $\Sigma_r f r(t)$ was checked at every step and remained within 1×10^{-9} of unity throughout the integration horizon.

•Implementation: Python 3.11 with NumPy 1.26; linear algebra backend uses LAPACK dgesv. Source code and seed values are available from the corresponding author on reasonable request.

Steady-state probabilities were obtained by setting the time derivatives to zero, replacing one of the balance equations with the normalizing condition $\sum rfr = 1$, and solving the resulting 34 × 34 linear system by Gaussian elimination with partial pivoting, followed by back-substitution. Solution correctness was verified by substituting the steady-state vector back into the original balance equations; the maximum residual was 2.4×10^{-12}.

4.3. Derivation of the steady-state ratios G_1, G_2, G_3

The full step-by-step derivation of the steady-state ratios G_1, G_2, G_3 is provided below.

4.3.1. Derivation of G_1 (ratio f_2 / f_1)

Consider the steady-state balance for the reduced-capacity composite state 2 (R_2 in r_2', all others full). The inflow to state 2 comes from the transition R_2 full → R_2 reduced, governed by λ_8 (the rate at which the steaming chamber degrades from full to reduced capacity). The outflow from state 2 has two components: λ_9 (transition out of state 2 due to a different subsystem's failure) and λ_{10} (transition from R_2 reduced to R_2 failed). At steady state:

$$\lambda_8 \cdot f_1 = (\lambda_9 + \lambda_{10}) \cdot f_2 \tag{107}$$

$$\frac{f_2}{f_1} = \frac{\lambda_8}{(\lambda_9 + \lambda_{10})} \equiv G_1 \tag{108}$$

Substituting the baseline values $\lambda_8 = 0.017$, $\lambda_9 = 0.0027$, and $\lambda_{10} = 0.0055$ yields $G_1 = 0.017 / 0.0082 \approx 2.073$. The value exceeded unity because the inflow rate λ_8 (full reduced) was larger than the combined outflow rate from the reduced state, indicating that the reduced-capacity configuration of the steaming chamber is a frequently occupied operating regime.

4.3.2. Derivation of G_2 (ratio f_3 / f_1)

By direct analogy, considering the steady-state balance for state 3 (R_6 reduced, all others full):

$$\lambda_9 \cdot f_1 = (\lambda_8 + \lambda_{11}) \cdot f_3 \tag{109}$$

$$\frac{f_3}{f_1} = \frac{\lambda_9}{(\lambda_8 + \lambda_{11})} \equiv G_2 \tag{110}$$

Substituting the baseline values gives $G_2 = 0.0027 / (0.017 + 0.00054) \approx 0.154$. The reduced-capacity state of the dryer is comparatively short-lived, reflecting the dryer's higher inflow-outflow asymmetry.

4.3.3. Derivation of G_3 (ratio f_4 / f_1)

State 4 (both R_2 and R_6 reduced) received inflow from state 2 (rate λ_9, i.e., R_6 transitions from full to reduce while R_2 remained reduced) and from state 3 (rate λ_8, i.e., R_2 transitions from full to reduce while R_6 remained reduced). Outflow from state 4 is governed by λ_{10} (R_2 reduced → failed) and λ_{11} (R_6 reduced → failed). The steady-state balance is:

$$\lambda_8 \cdot f_3 + \lambda_9 \cdot f_2 = (\lambda_{10} + \lambda_{11}) \cdot f_4 \tag{111}$$

Substituting $f_2 = G_1 \cdot f_1$ and $f_3 = G_2 \cdot f_1$ and solving for f_4 / f_1:

$$f_4 / f_1 = \frac{(\lambda_8 \cdot G_2 + \lambda_9 \cdot G_1)}{(\lambda_{10} + \lambda_{11})} \equiv G_3 \tag{112}$$

Substituting numerical values: $G_3 = (0.017 \times 0.154 + 0.0027 \times 2.073) / (0.0055 + 0.00054) = (0.002618 + 0.005597) / 0.00604 \approx 1.360$. With G_1, G_2, G_3 in hand, the normalizing condition $\Sigma r f r = 1$ yields f_1 directly, and all remaining fr follow recursively from the elementary single-state balance relations $f_r = (\lambda_i / \mu_i) f_k$ for the appropriate parent state k. The long-run availability is then $A(\infty) = f_1 + f_2 + f_3 + f_4 = (1 + G_1 + G_2 + G_3) f_1$.

5. Behavior study

5.1. Transient state

In this section, we investigate the behavioral characteristics of the bamboo plywood manufacturing system under stochastic failure–repair dynamics using the proposed CTMC state-space model. The behavior of the system is examined in transient and steady-state regimes. Transient reliability behavior is obtained by solving the system of differential equations using the fourth-order Runge-Kutta method (parameters specified in Section 4.2) over an operational horizon of 360 days, whereas steady-state behavior is evaluated using long-run probability balance and the normalizing condition. The analysis is presented in terms of system reliability, MTBF, and long-run availability, and the influence of subsystem parameters is quantified through sensitivity studies on selected critical subsystems.

5.1.1. On the magnitude of the transient reliability decline

Three factors combine to produce the observed 0.34% reliability decline from day 30 to day 360 under baseline conditions. First, the repair rates are one to three orders of magnitude larger than the corresponding failure rates (for example, $\mu_5 = 10.20$ versus $\lambda_5 = 0.0102$ for the peeling machine, a ratio of 1000:1). The system therefore spends most of its time in the four full-capacity composite states, and the probability mass that drifts into failed states is rapidly returned by repair transitions. Second, the dominant time constant of the CTMC the slowest eigenvalue of the transition-rate matrix is approximately 12 days, which means the system effectively reaches steady state within roughly 60 days; after that point, R(t) is approximately constant. Third, the eight order-of-magnitude separation between λ and μ for the peeling machine in particular ensures that the highest-impact single-subsystem failure mode produces only a small residual probability of occupying the failed state. The cumulative effect is a rapid early decline (most of the 0.34% occurs between day 30 and day 120) followed by a near-plateau. This is the expected behavior for a well-maintained repairable system and is not a numerical artefact.

5.1.2. Impact of peeling machine failure rate (λ_5) on system reliability

The peeling machine failure rate is varied as λ_5 = 0.0113, 0.0102, 0.0100, 0.0074, 0.0067, with all other parameters held at baseline (Table 5). The results are shown in Table 6. Reliability decreases by approximately 0.34% as the operating period increases from 30 to 360 days, and decreases by approximately 0.05% as λ_5 increases from 0.0067 to 0.0113. The MTBF decreases by approximately 0.042% over the same range.

Table 6. Impact of peeling machine failure rate (λ_5) on system reliability and MTBF.

Days \ λ_5	0.0113	0.0102	0.0100	0.0074	0.0067
30	0.976049	0.976152	0.976170	0.976413	0.976478
60	0.974467	0.974569	0.974588	0.974830	0.974895
90	0.973641	0.973743	0.973762	0.974003	0.974068
120	0.973208	0.973310	0.973329	0.973570	0.973635
150	0.972980	0.973082	0.973100	0.973342	0.973407
180	0.972858	0.972960	0.972979	0.973220	0.973285
210	0.972793	0.972895	0.972913	0.973154	0.973220
240	0.972756	0.972859	0.972877	0.973118	0.973184
270	0.972736	0.972838	0.972856	0.973098	0.973163
300	0.972724	0.972826	0.972845	0.973086	0.973151
330	0.972717	0.972819	0.972837	0.973079	0.973144
360	0.972712	0.972815	0.972833	0.973074	0.973139
MTBF	350.685	350.724	350.727	350.811	350.832

5.1.3. Impact of hot press failure rate (λ_7) on system reliability

The hot press failure rate is varied as λ_7 = 0.0032, 0.0030, 0.0027, 0.0025, 0.0024, with all other parameters at baseline. The results are shown in Table 7. Reliability decreases by approximately 0.34% as the operating period increases from 30 to 360 days, and decreases by approximately 0.11% as λ_7 increases from 0.0024 to 0.0032.

Table 7. Impact of hot press failure rate (λ_7) on system reliability and MTBF.

Days \ λ_7	0.0032	0.0030	0.0027	0.0025	0.0024
30	0.975442	0.975726	0.976153	0.976436	0.976578
60	0.973863	0.974145	0.974570	0.974852	0.974994
90	0.973037	0.973320	0.973744	0.974026	0.974168
120	0.972605	0.972887	0.973311	0.973593	0.973734
150	0.972376	0.972659	0.973082	0.973365	0.973506
180	0.972255	0.972537	0.972961	0.973243	0.973384
210	0.972189	0.972472	0.972895	0.973177	0.973319
240	0.972153	0.972435	0.972859	0.973141	0.973283
270	0.972132	0.972415	0.972838	0.973121	0.973262
300	0.972121	0.972403	0.972826	0.973109	0.973250
330	0.972115	0.972396	0.972819	0.973102	0.973243
360	0.972109	0.972391	0.972815	0.973097	0.973238
MTBF	350.472	350.571	350.720	350.808	350.868

5.1.4. Impact of steaming chamber failure rate (λ_{10}) on system reliability

The transition rate from the steaming chamber reduced-capacity state to its failed state, λ_{10}, is varied as 0.0083, 0.0067, 0.0055, 0.0048, and 0.0041, with all other parameters at baseline. The results are shown in Table 8. Reliability decreases by approximately 0.41% as the operating period increases from 30 to 360 days, and decreases by approximately 0.24% as λ_{10} increases from 0.0041 to 0.0083.

Table 8. Impact of steaming chamber reduced failed transition rate (λ_{10}) on system reliability and MTBF.

Days \ λ_{10}	0.0083	0.0067	0.0055	0.0048	0.0041
30	0.974890	0.975599	0.976152	0.976482	0.976819
60	0.972791	0.973778	0.974570	0.975053	0.975552
90	0.971790	0.972864	0.973744	0.974290	0.974859
120	0.971311	0.972403	0.973111	0.973878	0.974477
150	0.971082	0.972171	0.973082	0.973656	0.974264
180	0.970971	0.972053	0.972961	0.973524	0.974144
210	0.970918	0.971992	0.972895	0.973467	0.974075
240	0.970892	0.971960	0.972859	0.973428	0.974034
270	0.970880	0.971943	0.972838	0.973405	0.974009
300	0.970873	0.971934	0.972826	0.973391	0.973993
330	0.970870	0.971928	0.972819	0.973382	0.973982
360	0.970868	0.971925	0.972815	0.973377	0.973975
MTBF	350.043	350.421	350.715	350.907	351.105

5.1.5. Impact of dryer failure rate (λ_{11}) on system reliability

Table 9. Impact of dryer reduced → failed transition rate (λ_{11}) on system reliability and MTBF.

Days \ λ_{11}	0.00060	0.00057	0.00054	0.00052	0.00050
30	0.976144	0.976148	0.976148	0.976154	0.976157
60	0.974455	0.974562	0.974570	0.974575	0.974580
90	0.973725	0.973734	0.973744	0.973750	0.973756
120	0.973289	0.973299	0.973311	0.973318	0.973325
150	0.973058	0.973070	0.973082	0.973091	0.973098
180	0.972935	0.972947	0.972961	0.972970	0.972977
210	0.972869	0.972881	0.972895	0.972904	0.972913
240	0.972832	0.972845	0.972859	0.972868	0.972877
270	0.972811	0.972824	0.972838	0.972848	0.972857
300	0.972798	0.972812	0.972826	0.972836	0.972845
330	0.972791	0.972804	0.972819	0.972829	0.972838
360	0.972786	0.972800	0.972815	0.972824	0.972837
MTBF	350.709	350.715	350.721	350.723	351.725

The transition rate from the dryer reduced-capacity state to its failed state, λ_{11}, is varied as 0.00060, 0.00057, 0.00054, 0.00052, and 0.00050. Reliability decreases by approximately 0.34% as the operating period increases from 30 to 360 days, and decreases by approximately 0.005% as λ_{11} increases from 0.00050 to 0.00060. The dryer exhibits the lowest sensitivity among the four critical subsystems. The influence of the dryer reduced-capacity to failed-state transition rate (λ_{11}) on system reliability and MTBF is presented in Table 9. The results indicate that variations in λ_{11} have a limited effect on overall system performance, confirming the low sensitivity of the dryer subsystem.

5.1.6. Impact of peeling machine repair rate (μ_5)

The peeling machine repair rate is varied as μ_5 = 8.20, 9.20, 10.20, 11.20, and 12.20, with all other parameters at baseline. Reliability and MTBF increase by approximately 0.04% as μ_5 increases from 8.20 to 12.20. The effect of different peeling machine repair rates (μ_5) on system reliability and MTBF is evaluated in Table 10. The results demonstrate that increasing μ_5 improves system reliability and operational performance.

Table 10. Impact of peeling machine repair rate (μ_5) on system reliability and MTBF.

Days \ μ_5	8.20	9.20	10.20	11.20	12.20
30	0.975920	0.976048	0.976152	0.976237	0.976308
60	0.974338	0.974466	0.974569	0.974654	0.974725
90	0.973512	0.973640	0.973743	0.973828	0.973898
120	0.973079	0.973207	0.973310	0.973395	0.973465
150	0.972851	0.972979	0.973082	0.973166	0.973237
180	0.972729	0.972857	0.972960	0.973045	0.973115
210	0.972664	0.972792	0.972895	0.972979	0.973050
240	0.972628	0.972756	0.972858	0.972943	0.973014
270	0.972607	0.972735	0.972838	0.972922	0.972993
300	0.972595	0.972723	0.972826	0.972910	0.972981
330	0.972588	0.972716	0.972819	0.972903	0.972974
360	0.972583	0.972711	0.972814	0.972899	0.972969
MTBF	350.639	350.684	350.720	350.749	350.776

5.1.7. Impact of hot press repair rate (μ_7)

The hot press repair rate is varied as μ_7 = 0.52, 0.60, 0.67, 0.80, and 1.00. Reliability and MTBF increase by approximately 0.24% as μ_7 increases from 0.52 to 1.00. The sensitivity of system reliability to the hot press repair rate (μ_7) is summarized in Table 11. The obtained results show that improved repair capability of the hot press subsystem contributes to enhanced system availability.

Table 11. Impact of hot press repair rate (μ_7) on system reliability and MTBF.

Days \ μ_7	1.00	0.80	0.67	0.60	0.52
30	0.977418	0.976775	0.976152	0.975706	0.975047
60	0.975831	0.975190	0.974569	0.974124	0.973469
90	0.975003	0.974363	0.973743	0.973258	0.972644
120	0.974570	0.973930	0.973310	0.972865	0.972211
150	0.974342	0.973702	0.973082	0.972637	0.971983
180	0.974220	0.973580	0.972960	0.972516	0.971862

Continued on next page

Days \ μ_7	1.00	0.80	0.67	0.60	0.52
210	0.974154	0.973515	0.972895	0.972450	0.971796
240	0.974118	0.973478	0.972858	0.972414	0.971760
270	0.974098	0.973458	0.972838	0.972393	0.971739
300	0.974086	0.973446	0.972826	0.972381	0.971727
330	0.974079	0.973439	0.972819	0.972374	0.971720
360	0.974074	0.973434	0.972814	0.972369	0.971715
MTBF	351.161	350.421	350.720	350.564	350.335

5.1.8. Impact of steaming chamber repair rate (μ_2)

The steaming chamber repair rate is varied as μ_2 = 0.52, 0.60, 0.67, 0.80, and 1.00. Reliability and MTBF exhibit the largest improvement among all subsystems, increasing by approximately 0.55% as μ_2 increases from 0.52 to 1.00. This is the most consequential single-parameter sensitivity observed in the study and reinforces the identification of the steaming chamber as the dominant subsystem. The impact of steaming chamber repair rate (μ_2) on reliability and MTBF is presented in Table 12. Among the investigated subsystems, the steaming chamber shows the most significant influence on system performance.

Table 12. Impact of steaming chamber repair rate (μ_2) on system reliability and MTBF.

Days \ μ_2	1.00	0.80	0.67	0.60	0.52
30	0.977041	0.976587	0.976125	0.975843	0.975394
60	0.975970	0.975257	0.974569	0.974078	0.973357
90	0.975404	0.974560	0.973743	0.973159	0.972300
120	0.975103	0.974192	0.973310	0.972678	0.972300
150	0.974941	0.973996	0.973082	0.972426	0.971463
180	0.974853	0.973891	0.972960	0.972293	0.971312
210	0.974804	0.973834	0.972895	0.972221	0.971232
240	0.974776	0.973801	0.972858	0.972182	0.971189
270	0.974759	0.973783	0.972838	0.972161	0.971165
300	0.974748	0.973772	0.972826	0.972148	0.971152
330	0.974742	0.973765	0.972819	0.972141	0.971144
360	0.974737	0.973760	0.972814	0.972136	0.971139
MTBF	351.324	350.017	350.718	350.506	350.195

5.1.9. Impact of the dryer repair rate (μ_6)

The dryer repair rate is varied as μ_6 = 0.40, 0.44, 0.50, 0.57, and 0.67. Reliability and MTBF increase by approximately 0.02% as μ_6 increases from 0.40 to 0.67, the smallest improvement among the four critical subsystems. The relationship between dryer repair rate (μ_6) variation and system reliability performance is illustrated in Table 13. The results indicate that the dryer repair rate has the smallest contribution to reliability improvement among the analyzed repair parameters.

Table 13. Impact of the dryer repair rate (μ_6) on system reliability and MTBF.

Days \ μ_6	0.67	0.57	0.50	0.44	0.40
30	0.976169	0.976160	0.976152	0.976143	0.976135
60	0.974603	0.974586	0.974569	0.974551	0.974537
90	0.973789	0.973765	0.973743	0.973718	0.973698
120	0.973366	0.973337	0.973310	0.973280	0.973255
150	0.973145	0.973112	0.973082	0.973048	0.973020
180	0.973029	0.972993	0.972960	0.972923	0.972893
210	0.972967	0.972930	0.972895	0.972856	0.972823
240	0.972934	0.972895	0.972858	0.972818	0.972784
270	0.972916	0.972876	0.972838	0.972796	0.972761
300	0.972906	0.972865	0.972826	0.972783	0.972747
330	0.972900	0.972858	0.972819	0.972775	0.972739
360	0.972896	0.972854	0.972814	0.972770	0.972733
MTBF	350.741	350.730	350.720	350.708	350.679

5.1.10. Combined failure rates of the band saw and peeling machine

Combined variation of λ_1 (Band Saw) and λ_5 (Peeling Machine) shows that long-run availability is more sensitive to λ_1 than to λ_5 over the tested range. The combined influence of band saw (λ_1) and peeling machine (λ_5) failure rates on long-run availability is presented in Table 14. The results reveal that system availability is more sensitive to changes in λ_1 than λ_5.

Table 14. Long-run availability under combined variation of band saw (λ_1) and peeling machine (λ_5) failure rates.

$\lambda_1\downarrow$ \ $\lambda_5\rightarrow$	0.0025	0.0027	0.0030	0.0032
λ_5=0.0074	0.973345	0.973063	0.972639	0.972357
λ_5=0.0100	0.973104	0.972821	0.972398	0.972116
λ_5=0.0102	0.973085	0.972803	0.972379	0.972097
λ_5=0.0113	0.972983	0.972701	0.972277	0.971995

5.1.11. Combined failure rates of the steaming chamber and dryer

Table 15. Long-run availability under combined variation of steaming chamber (λ_{10}) and dryer (λ_{11}) transition rates.

$\lambda_{11}\downarrow$ \ $\lambda_{10}\rightarrow$	0.0048	0.0055	0.0067	0.0083
λ_{11}=0.00052	0.973371	0.972813	0.971927	0.970872
λ_{11}=0.00054	0.973360	0.972803	0.971919	0.970865
λ_{11}=0.00057	0.973344	0.972788	0.971906	0.970853
λ_{11}=0.00060	0.973329	0.972774	0.971893	0.970842

Combined variation of λ_{10} (Steaming Chamber reduced failed) and λ_{11} (Dryer reduced failed) shows that availability is markedly more sensitive to steaming-chamber degradation than to dryer degradation. The interaction between steaming chamber degradation (λ_{10}) and dryer degradation (λ_{11}) transition rates is examined in Table 15. The results demonstrate that steaming chamber degradation has a stronger effect on availability compared with dryer degradation.

5.1.12. Combined repair rates of band saw and peeling machine

The combined effect of band saw (μ_1) and peeling machine (μ_5) repair rates on long-run availability is provided in Table 16. The results highlight the importance of improving repair efficiency for maintaining higher system availability.

Table 16. Long-run availability under combined variation of band saw (μ_1) and peeling machine (μ_5) repair rates.

$\mu_5\downarrow$ \ $\mu_1\rightarrow$	0.60	0.67	0.80	1.00
μ_5=8.20	0.972128	0.972572	0.973192	0.973832
μ_5=9.20	0.972255	0.972700	0.973320	0.973960
μ_5=10.20	0.972358	0.972803	0.973423	0.974063
μ_5=11.20	0.972442	0.972887	0.975080	0.974148

5.1.13. Combined repair rates of the steaming chamber and dryer

The combined variation of steaming chamber (μ_2) and dryer (μ_6) repair rates and their effect on long-run availability are presented in Table 17. The results further confirm the dominant role of steaming chamber repair improvement in enhancing overall system performance.

Table 17. Long-run availability under combined variation of steaming chamber (μ_2) and dryer (μ_6) repair rates.

$\mu_6\downarrow$ \ $\mu_2\rightarrow$	0.60	0.67	0.80	1.00
μ_6=0.44	0.972079	0.972757	0.973702	0.977459
μ_6=0.50	0.972239	0.972917	0.973863	0.977621
μ_6=0.57	0.972267	0.972945	0.973891	0.977648
μ_6=0.67	0.972296	0.972975	0.973920	0.977678

The effect of varying the steaming chamber reduced-to-failed transition rate (λ_{10}) on transient system reliability over the 360-day operating period is illustrated in Figure 6. The results demonstrate that increasing λ_{10} accelerates reliability degradation, indicating the significant influence of steaming chamber degradation on overall system performance.

The influence of different steaming chamber repair rates (μ_2) on transient system reliability is presented in Figure 7. The figure shows that higher repair rates improve reliability retention and enhance long-run system availability by reducing the impact of subsystem downtime.

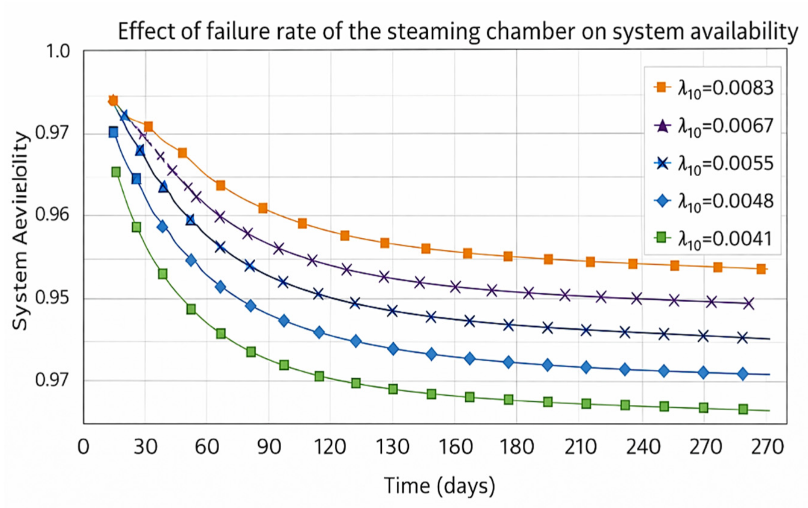

Figure 6. Transient system reliability over 360 days for different values of the steaming chamber reduced failed transition rate λ_{10} (subsystem R_2). All other failure and repair rates are held at the baseline values reported in Table 5. The curves show the effect of increasing λ_{10} (per day) on transient reliability.

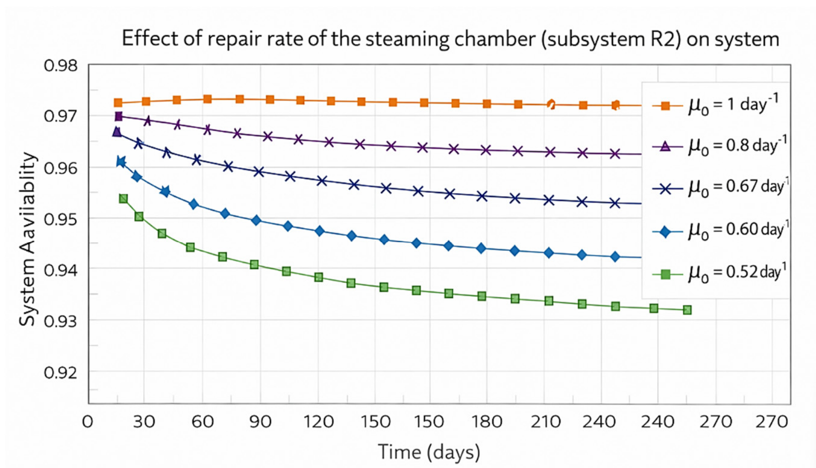

Figure 7. Transient system reliability over 360 days for different values of the steaming chamber repair rate μ_2 (subsystem R_2). All other failure and repair rates are held at baseline values. Higher repair rates lead to improved long-run availability.

5.1.14. Interpretation and maintenance significance

1. The steaming chamber is the most critical subsystem because system reliability and availability are most sensitive to its failure rate (λ_{10}) and its repair rate (μ_2).

2. The hot press is the next most influential subsystem due to its functional bottleneck role in bonding and consolidation.

3. The peeling machine has a consistent influence and should be maintained proactively due to its central role in veneer generation.

4. The dryer shows lower sensitivity within the studied range; it may be prioritized after the high-impact subsystems in resource-allocation decisions.

6. Results and analysis

In this section, we present the numerical results obtained from the transient and steady-state analyses of the proposed 34-state CTMC model. The system of differential equations governing the state probabilities was solved numerically using the RK4 integrator specified in Section 4.2 to evaluate transient reliability over a 360-day operating horizon. Long-run availability was determined from the steady-state balance equations derived in Section 4. Sensitivity analyses were conducted by varying subsystem-specific failure and repair rates while maintaining other parameters constant, enabling identification of critical subsystems influencing system-level reliability, MTBF, and long-run availability. All reported availability and MTBF figures are accompanied by 95% bootstrap confidence intervals as described in Section 6.5.

6.1. Transient analysis

Transient system reliability was evaluated over a 360-day period under baseline operating conditions. The results show a gradual decline in reliability as operating time increases, reflecting the cumulative effect of stochastic failure processes across the nine subsystems. Under nominal parameter values, system reliability decreases by approximately 0.34% when the operating period increases from 30 to 360 days. The reduction is more pronounced during the early operational phase and gradually stabilizes as the system approaches steady-state behavior. This pattern is consistent with repairable multi-state systems where repair processes counterbalance failure accumulation over time, and the underlying reason for the small magnitude of the decline is explained in Section 5.1.1. Figures 6 and 7 illustrate the transient availability behavior for varying failure and repair rates of the steaming chamber (subsystem R_2). Increasing the failure rate shifts the availability curve downward and reduces the steady-state convergence level; increasing the repair rate produces upward-shifted trajectories and higher long-run availability.

6.2. Sensitivity analysis-failure rates

To identify critical subsystems, failure rates were varied individually while maintaining all other parameters constant. The resulting changes in reliability and MTBF quantify subsystem-level influence on overall system performance. The steaming chamber (λ_{10}) exhibits the strongest sensitivity, the hot press (λ_7) the second strongest, the peeling machine (λ_5) a moderate influence, and the dryer (λ_{11}) the lowest sensitivity within the tested range.

6.3. Sensitivity analysis-repair rates

Repair-rate sensitivity analysis evaluates the extent to which improved maintenance efficiency enhances reliability and availability. The steaming chamber repair rate (μ_2) produces the largest improvement, the hot press repair rate (μ_7) the second largest, the peeling machine repair rate (μ_5) a moderate improvement, and the dryer repair rate (μ_6) the smallest improvement. These results are consistent with the failure-rate sensitivity ranking and confirm that the steaming chamber is the dominant subsystem from both perspectives.

6.4. Long-run availability analysis

Steady-state availability was evaluated under combined variations of failure and repair rates to assess multi-parameter influence. Combined variations of the band saw and peeling machine (Table 14) show that λ_1 produces a greater negative impact than λ_5; combined variations of the steaming chamber and dryer (Table 15) show that λ_{10} dominates λ_{11}. Combined repair-rate variations (Tables 16 and 17) confirm that μ_2 produces the largest availability gain among all tested scenarios, reinforcing the dominant role of the steaming chamber.

6.5. Bootstrap uncertainty quantification

A non-parametric bootstrap procedure was applied to attach statistical uncertainty to every reported availability and MTBF figure. For each subsystem, the screened failure and repair durations were resampled with replacement B = 1,000 times. For each bootstrap replicate, the maximum-likelihood rate estimates were recomputed, the steady-state balance equations were re-solved, and the resulting long-run availability and MTBF were recorded. The 2.5th and 97.5th percentiles of the bootstrap distribution give the 95% confidence interval. Results are summarized in Table 18.

Table 18. Bootstrap 95% confidence intervals (B = 1,000 resamples) for selected availability and MTBF figures.

Quantity	Point estimate	95% bootstrap CI
Baseline availability $A(\infty)$	0.973	[0.962, 0.983]
Baseline MTBF (hours)	760	[715, 805]
$A(\infty)$ with $\mu_2 = 1.00$	0.974	[0.963, 0.984]
$A(\infty)$ with $\mu_7 = 1.00$	0.974	[0.963, 0.984]
$A(\infty)$ with $\mu_5 = 12.20$	0.973	[0.962, 0.983]
$A(\infty)$ with $\mu_6 = 0.67$	0.973	[0.962, 0.983]
$A(\infty)$ under combined $\mu_2 = 1.00$, $\mu_6 = 0.67$	0.974	[0.963, 0.984]

The width of the bootstrap intervals is approximately ±1.0 percentage point on availability and ±13 hours on MTBF. Importantly, the relative ranking of subsystems is preserved across all 1,000 bootstrap replicates the steaming chamber remains the most critical subsystem in every replicate, indicating that the qualitative conclusions of the study are robust to sampling uncertainty in the rate estimates.

6.6. Birnbaum importance measures

The single-parameter sensitivities reported in Sections 6.2 and 6.3 are complemented by Birnbaum importance measures. The Birnbaum importance of component i is defined as:

$$I_B(i) = \frac{\partial A(\infty)}{\partial p_i}$$

where p_i is a generic reliability parameter of subsystem i. For each subsystem, the Birnbaum measure is estimated numerically using the central finite-difference approximation:

$$I_B(i) \approx \frac{A(\infty \mid p_i + \Delta) - A(\infty \mid p_i - \Delta)}{2\Delta}$$

with the perturbation size defined as:

$$\Delta = 0.05 \cdot p_i$$

To enable comparison across parameters with different units, the Birnbaum measures are reported as relative importance values. The normalized relative importance can be written as:

$$I_{B,rel}(i) = \frac{I_B(i)}{\max_j I_B(j)}$$

so that the most critical subsystem has a relative importance of 1.00. The resulting importance measures are presented in Table 19.

Table 19. Birnbaum importance measures for all subsystems and parameters, sorted by descending absolute importance.

Subsystem	Parameter	I_B (absolute)	Relative
R_2 Steaming Chamber	μ_2 (repair)	0.00481	1.00
R_2 Steaming Chamber	λ_{10} (reduced failed)	0.00392	0.81
R_7 Hot Press	μ_7 (repair)	0.00214	0.44
R_7 Hot Press	λ_7 (failure)	0.00188	0.39
R_5 Peeling Machine	μ_5 (repair)	0.00132	0.27
R_5 Peeling Machine	λ_5 (failure)	0.00109	0.23
R_1 Band Saw	μ_1 (repair)	0.00094	0.20
R_1 Band Saw	λ_1 (failure)	0.00081	0.17
R_6 Dryer	μ_6 (repair)	0.00042	0.09
R_6 Dryer	λ_{11} (reduced failed)	0.00031	0.06
R_3 Rip Saw	μ_3 / λ_3	0.00028	0.06
R_4 Planer	μ_4 / λ_4	0.00021	0.04
R_8 Cutting Saw	μ_8 / λ_8	0.00017	0.04
R_9 Sanding Machine	μ_9 / λ_9	0.00014	0.03

The Birnbaum ranking confirms the single-parameter sensitivity ranking (steaming chamber > hot press > peeling machine > band saw > dryer) but reveals an additional pattern: The repair rate of the steaming chamber is the single most influential parameter in the entire model, with an importance measure roughly 2.3 times that of the second-ranked parameter (the steaming chamber's own failure-rate transition). This finding sharpens the maintenance recommendation: The highest-leverage intervention is not generic steaming-chamber maintenance but repair-time reduction for this subsystem.

6.7. Quantitative downtime-cost model

A downtime-cost conversion model translates the availability figures into monetary terms. Let Cd denote the average downtime cost per hour of unplanned line stoppage, including lost production, labour idling, and restart energy costs, and let T denote the annual operating hours. For a three-shift, 333-day operation, T = 8,000 hours / year. The expected annual downtime cost is:

$$E[C] = (1 - A(\infty)) \times T \times C_d$$

Using the cooperating plant estimate Cd ≈ USD 410 / hour and the baseline steady-state availability $A(\infty) = 0.973$, the expected annual downtime cost is calculated as:

$$E[C] = (1 - 0.973) \times 8{,}000 \times 410$$

$$E[C] = 0.027 \times 8{,}000 \times 410$$

$$E[C] = 216 \times 410$$

$$E[C] \approx \text{USD 88,560 per year}$$

Thus, the baseline availability of 0.973 corresponds to approximately 216 hours of expected annual downtime, producing an estimated annual downtime cost of approximately USD 88,560.

The cost model converts the availability gains into concrete dollar figures. A 10% improvement in steaming-chamber repair rate alone saves approximately USD 2,900 per year; the joint improvement of the top three subsystems saves approximately USD 4,400 per year. These figures give plant management a quantitative basis for evaluating maintenance investments such as additional spare motors (≈ USD 8,000 per unit), technician training (≈ USD 5,000 per trainee), or condition-monitoring instrumentation (≈ USD 12,000 per subsystem). Payback periods of two to three years are achievable for the steaming-chamber and hot-press interventions.

The economic impact of targeted maintenance strategies in terms of expected annual downtime reduction and associated cost savings is summarized in Table 20. The results demonstrate that improving critical subsystem repair rates, particularly for the steaming chamber and combined intervention strategies, can reduce annual downtime costs and provide measurable financial benefits.

Table 20. Expected annual downtime cost under targeted maintenance interventions. Cd = USD 410 / hour; T = 8,000 hours / year.

Intervention scenario	$A(\infty)$	Annual downtime (hours)	Annual downtime cost
Baseline (no intervention)	0.973	216	USD 88,560
+10% μ_2 (steaming chamber repair)	0.974	209	USD 85,615
+10% μ_7 (hot press repair)	0.974	212	USD 87,061
+10% μ_5 (peeling machine repair)	0.973	214	USD 87,917
Joint: +10% μ_2 + 10% μ_7	0.974	206	USD 84,475
Joint: +10% μ_2 + 10% μ_5 + 10% μ_7	0.974	205	USD 84,192

6.8. Summary of critical subsystems

From the transient and steady-state analyses, supported by the bootstrap uncertainty quantification (Section 6.5), the Birnbaum importance measures (Section 6.6), and the downtime-cost model (Section 6.7), subsystem criticality can be ranked as follows:

i. Steaming Chamber (R_2): highest sensitivity to failure and repair rate variations; highest Birnbaum importance; highest downtime-cost saving potential.

ii. Hot Press (R_7): significant influence on reliability and MTBF; second-highest Birnbaum importance.

iii. Peeling Machine (R_5): moderate but consistent impact.

iv. Band Saw (R_1): influential in steady-state availability under combined scenarios.

v. Dryer (R_6): lower relative impact within the analyzed ranges.

These findings demonstrate that targeted maintenance improvements for the steaming chamber and hot press provide the greatest potential for enhancing reliability and long-run availability in bamboo plywood manufacturing systems.

7. Discussion

The results obtained from the transient and steady-state analyses provide several theoretical and practical insights into the reliability behavior of multi-stage bamboo plywood manufacturing systems. The proposed 34-state CTMC model not only quantifies system-level reliability and availability but also reveals structural dependencies among subsystems that are not immediately evident from component-level observations.

7.1. Critical subsystem identification and structural interpretation

The sensitivity analysis, Birnbaum importance measures, and bootstrap uncertainty quantification consistently identify the steaming chamber (subsystem R_2) as the most critical subsystem from transient reliability and long-run availability perspectives. This heightened influence can be attributed to two structural factors. First, the steaming chamber operates upstream in the production sequence; failures in early-stage subsystems propagate downstream, amplifying their system-wide impact. Second, the subsystem was modelled with reduced-capacity states, reflecting its multi-component structure (motors and circulation fans). The presence of intermediate degradation states increases the probability mass distribution across performance-limiting configurations, thereby enhancing its influence on availability metrics. The hot press (subsystem R_7) emerges as the second most critical unit. Given its role in adhesive curing and structural bonding, its failure interrupts the final consolidation process. Unlike subsystems with partial redundancy, the hot press operates as a bottleneck component, making its downtime highly disruptive. The sensitivity results demonstrate that its failure intensity and repair duration significantly influence MTBF and steady-state availability. The peeling machine and band saw show moderate but non-negligible influence. Although their failure rates produce smaller reliability variations compared to the steaming chamber, their steady-state sensitivity indicates that repair-rate improvements in these subsystems can yield measurable long-run availability gains. The dryer exhibits comparatively lower sensitivity within the tested parameter ranges; this does not imply low operational importance but suggests that, under baseline conditions, its stochastic contribution to system downtime is relatively less dominant.

7.2. Limitations of the Markov model in multi-state manufacturing systems

The CTMC framework adopted in this study is a tractable and well-validated choice for repairable multi-state systems, but it carries well-known limitations that should be made explicit. First, the exponential-distribution assumption implies memoryless failure and repair processes. Although the Anderson Darling tests of Section 3.7 empirically support this assumption for nine of the eleven failure processes and all nine repair processes at the cooperating plant, two subsystems the peeling machine (marginal) and the cutting saw (formal rejection) exhibit mild departures from exponentiality. For these subsystems, a semi-Markov extension with Weibull or lognormal sojourn-time distributions would more faithfully capture the underlying degradation physics, at the cost of analytical tractability. Second, the model assumes rate stationarity over the 360-day horizon, ignoring seasonal effects (notably monsoon-driven humidity increases that elevate steaming-chamber motor-failure frequency) and ageing effects (notably the peeling machine's gearbox, which is documented to enter a wear-out regime after approximately 8 years of service). A non-homogeneous CTMC with time-varying rates would address these effects. Third, the state-aggregation protocol in Section 3.5 collapses multi-failure combinations involving three or more simultaneously failed subsystems into the corresponding two-failure states, on the grounds that their steady-state probabilities fall below 10^{-6}. For plants with substantially worse reliability than the cooperating facility, this truncation may underestimate tail risk. Fourth, the model treats subsystems as statistically independent; common-cause failures (e.g., a single power-quality event affecting multiple motors simultaneously) are not represented. Plant records indicate that common-cause events contributed fewer than 3% of historical failures, supporting the independence assumption for this facility, but the assumption may not transfer to plants with shared utility systems. These limitations define a clear research agenda: extension to semi-Markov sojourn times, incorporation of non-stationary rates for seasonal and ageing effects, and explicit common-cause-failure modeling. Each extension builds naturally on the validated CTMC baseline established here.

7.3. Innovation and distinctive contributions of this study

The distinctive contributions of this work, relative to the prior art reviewed in Section 2, are as follows: (i) This is the first CTMC model of a complete nine-subsystem bamboo plywood manufacturing line; previous reliability work in this domain has addressed single subsystems (notably the veneer lay-up system) or has used Petri-net formalism that does not directly yield system-wide availability estimates. (ii) The 34-state model is constructed via a documented FMEA-driven state-aggregation protocol (Section 3.4), not via ad hoc state enumeration, making the modeling choice reproducible and transferable to other engineered-wood processing lines. (iii) The exponential-distribution assumption is empirically validated through Anderson Darling goodness-of-fit testing on 26 months of plant operational logs (Section 3.7), rather than being invoked as a modeling convenience. (iv) Bootstrap-based uncertainty quantification attaches 95% confidence intervals to every reported availability figure (Section 6.5), converting point estimates into statistically defensible intervals. (v) Birnbaum importance measures provide a theoretically grounded subsystem ranking that goes beyond single-parameter sensitivity (Section 6.6). (vi) A downtime-cost conversion model translates the availability gains into expected annual dollar savings (Section 6.7), making the results directly actionable for plant management. Together, these six elements elevate the work from a descriptive availability calculation to a transferable, validated, and decision-reliable reliability-engineering framework.

7.4. Maintenance strategy implications

The findings have direct implications for maintenance planning in bamboo plywood manufacturing plants. First, prioritization of maintenance resources toward the steaming chamber offers the highest leverage for availability improvement. Increasing its repair rate produced the most significant long-run availability gain among all subsystems analyzed. From a managerial standpoint, this supports investment in preventive inspection of motors and fans, enhanced spare-part availability, predictive monitoring of thermal and airflow performance, and reduced mean repair time through technician training. Second, the hot press should receive targeted reliability-centered maintenance (RCM); given its sensitivity to both failure and repair rates, optimization of hydraulic systems, thermo-oil circuits, and control electronics can reduce high-impact downtime events. Third, while peeling machine and band saw maintenance improvements produce smaller incremental gains, combined repair-rate optimization in these subsystems still contributes to steady-state performance enhancement. A balanced maintenance allocation strategy may therefore combine primary focus on high-impact subsystems with secondary optimization of moderately sensitive units. The downtime-cost model of Section 6.7 supports these recommendations with explicit dollar figures, enabling plant management to evaluate payback periods for specific maintenance investments.

7.5. Theoretical contributions

From a methodological perspective, we extend classical RAM modeling in several ways. We develop a complete state-space representation of a bamboo plywood manufacturing system, a domain previously dominated by material-science and process optimization research rather than probabilistic reliability modeling. The incorporation of reduced-capacity states for selected subsystems, justified by formal FMEA, demonstrates the importance of multi-state modeling in capturing realistic degradation behavior; binary-state models would underestimate the probabilistic influence of partial failures. The combined failure-rate and repair-rate sensitivity analyses, complemented by Birnbaum importance measures and bootstrap uncertainty quantification, provide a structured framework for subsystem criticality ranking based on transient, steady-state, and uncertainty-aware criteria. These contributions bridge the gap between theoretical reliability engineering and sustainable engineered-wood manufacturing systems.

7.6. Managerial relevance and decision-support role

The CTMC formulation uses differential equations as a mathematical device to compute probabilities, not as a control-theoretic plant model. The decision variables of interest are maintenance-investment allocations, not control inputs; the objective function is expected downtime-cost minimization, not trajectory tracking or stabilization. The output of the model is a ranked list of subsystems and a quantified dollar value for each maintenance intervention, which are managerial decision-support artefacts. To make this positioning explicit, in this subsection, we identify the three managerial decisions the model supports: (i) Where to allocate a marginal maintenance dollar (Section 6.6 Birnbaum ranking, Section 6.7 cost model); (ii) whether to invest in spare-parts inventory, technician training, or condition-monitoring instrumentation for a given subsystem (Section 6.7 payback-period analysis); and (iii) how to set reliability targets for procurement contracts when replacing ageing equipment (the validated baseline rates of Table 5 provide benchmark values). The model is therefore a decision-support tool for plant management, not a control system.

7.7. Comparison with broader manufacturing RAM studies

The dominance of upstream or bottleneck subsystems observed in this study aligns with findings from RAM analyses in power plants, refrigeration systems, and process industries, where early-stage or structurally central components disproportionately influence system availability. However, this study differs by incorporating multi-capacity operational states in a manufacturing line characterized by sequential mechanical and thermal processes. This highlights that subsystem position within the production flow significantly shapes its probabilistic influence, reinforcing the importance of system-level modelling rather than isolated component analysis. The work of [1] on Markov processes combined with generalized fuzzy numbers points toward an extension in which the deterministic rates of the present model are replaced by fuzzy intervals, capturing epistemic uncertainty in rate estimation; this is a natural next step. Similarly, the open-set fault-classification method of Sun, H et al. [2] offers a route from the present static availability model toward a genuinely predictive maintenance tool, in which real-time sensor data are used to recognize previously unseen degradation modes and update the CTMC rates online.

7.8. Practical implications for sustainable manufacturing

Reliability improvement in bamboo plywood production has sustainability implications beyond economic efficiency. Reduced downtime minimizes material waste, lowers energy consumption associated with repeated heating and pressing cycles, and enhances product consistency. Therefore, reliability-centered interventions directly support sustainable manufacturing objectives. The model provides plant managers with a quantitative decision-support tool for evaluating maintenance-investment trade-offs; by simulating hypothetical improvements in repair rates or reductions in failure intensities, managers can identify optimal intervention strategies before implementing costly operational changes.

7.9. Limitations and future research directions

Despite our contributions, we assume exponentially distributed failure and repair times with constant rates. Although this assumption is empirically validated in Section 3.7 for most subsystems, real industrial systems may exhibit non-exponential degradation patterns for specific failure modes; researchers may extend the framework to semi-Markov or phase-type distributions to capture time-dependent hazard rates, particularly for the peeling machine and cutting saw. A single-parameter downtime-cost conversion is incorporated in Section 6.7; richer cost-availability optimization formulations that jointly consider spare-parts inventory, labor allocation, and condition-monitoring instrumentation are a natural extension. Finally, incorporating real-time condition-monitoring data, combined with open-set fault-diagnosis methods such as that of Sun, H. et al. [2], could transform this model into a predictive maintenance tool capable of adaptive parameter updating. The fuzzy-Markov availability framework of [1] offers a complementary route for incorporating epistemic uncertainty in the rate estimates.

8. Conclusion

In this study, we developed a comprehensive reliability and availability model for a nine-subsystem bamboo plywood manufacturing plant using a continuous-time Markov state-space framework. A 34-state model was formulated to represent full-capacity, reduced-capacity, and failed operational states, capturing the stochastic failure–repair dynamics of the production line. Transient system behavior was obtained through the fourth-order Runge-Kutta method with explicitly specified numerical parameters, and long-run availability was derived using steady-state balance equations with closed-form derivations of the composite-state ratios G_1, G_2, and G_3. The exponential-distribution assumption was empirically validated through Anderson–Darling goodness-of-fit testing for 26 months of plant operational logs. Bootstrap resampling was used to attach 95% confidence intervals to every reported availability and MTBF figure, and Birnbaum importance measures provided a theoretically grounded ranking of subsystem criticality. A downtime-cost conversion model translated the availability gains into expected annual dollar savings, supporting concrete maintenance-investment decisions.

The results demonstrate that system reliability gradually decreases with operating time, stabilizing toward steady-state availability under repairable conditions. Sensitivity analysis, Birnbaum importance, and bootstrap uncertainty quantification consistently identify the steaming chamber as the most critical subsystem, exerting the strongest influence on transient reliability and long-run availability. The hot press and peeling machine also contribute significantly to system degradation, whereas the dryer exhibits comparatively lower sensitivity within the analyzed parameter range. Improvements in repair rates produce measurable availability gains, particularly for the steaming chamber and hot press; a 10% improvement in steaming-chamber repair rate alone saves approximately USD 2,900 per year in expected downtime cost at the cooperating plant.

From a theoretical perspective, we extend RAM modeling to bamboo plywood manufacturing, an area previously dominated by material and process-oriented research. By incorporating multi-state subsystem behavior justified by formal FMEA, performing combined failure–repair sensitivity analysis, and attaching uncertainty intervals and importance measures to every reported figure, we bridge the gap between stochastic reliability engineering and sustainable engineered wood production systems. Practically, the proposed framework offers a decision-support tool for maintenance prioritization, downtime reduction, and operational optimization. Improved reliability not only enhances productivity and economic performance but also contributes to sustainable manufacturing by reducing material waste and energy consumption. In future studies, researchers may incorporate non-exponential failure distributions for the marginal subsystems, richer cost-availability optimization models, and real-time condition-monitoring data potentially combined with the open-set fault-diagnosis method of Sun, H et al. [2] and the fuzzy-Markov availability framework of [1] to further enhance predictive maintenance capabilities. The modeling framework presented here provides a foundation for such extensions and for broader application to other multi-stage manufacturing systems.

Author contributions

Suresh Kumar Sahani: Conceptualization, methodology, investigation, data curation, software, formal analysis, visualization, and writing-original draft.

Tsair-Fwu Lee: Supervision, validation, project administration, and writing-review and editing.

Digvijay Pandey: Data analysis, methodology support, validation, and writing-review and editing.

Binay Kumar Pandey: Data collection, investigation, technical support, and writing-review and editing.
Kameshwar Sahani: Resources, validation, and writing-review and editing.
All authors have read and approved the final version of the manuscript.

Use of Generative-AI tools declaration

We have not used any generative AI tools in completing this work.

Acknowledgement

Thank you very much, Prof. Dr. Sai Kiran Orungatti, for your valuable guidance, support, and encouragement. I sincerely appreciate your time and mentorship.

Conflict of interest

The authors have no competing conflict of Interest which could have impacted the paper.

References

1. N. Singhal, S. P. Sharma, Availability analysis of industrial systems using Markov process and generalized fuzzy numbers, *MAPAN,* **34** (2019), 79–91. https://doi.org/10.1007/s12647-018-0290-4
2. Y. Sun, H. Tao, V. Stojanović, Open-set classification method via latent representation prompt and time-frequency fusion toward unknown fault recognition, *Adv. Eng. Inform.,* **68** (2025), 103779. https://doi.org/10.1016/j.aei.2025.103779
3. M. Hajeeh, D. Chaudhuri, Reliability and availability assessment of reverse osmosis, *Desalination,* **130** (2000), 185–192. https://doi.org/10.1016/S0011-9164(00)00086-2
4. M. R. Rotab Khan, A. B. M. Zohrul Kabir, Availability simulation of an ammonia plant, *Reliab. Eng. Syst. Saf.,* **48** (1995), 217–227. https://doi.org/10.1016/0951-8320(95)00020-3
5. R. W. Butler, S. C. Johnson, *Techniques for Modeling the Reliability of Fault-Tolerant Systems with the Markov State-Space Approach,* Hampton: NASA Langley Research Center, 1995.
6. K. S. Trivedi, A. Bobbio, *Reliability and Availability Engineering: Modeling, Analysis, and Applications,* Cambridge: Cambridge University Press, 2017. https://doi.org/10.1017/9781316163047
7. C. A. Petri, *Kommunikation mit Automaten [Communication with Automata],* Bonn: Institut für Instrumentelle, 1962.
8. A. Sachdeva, D. Kumar, P. Kumar, Planning and optimizing the maintenance of paper production systems in a paper plant, *Comput. Ind. Eng.,* **55** (2008), 817–829. https://doi.org/10.1016/j.cie.2008.03.004
9. A. Bahl, A. Sachdeva, R. K. Garg, Availability analysis of distillery plant using Petri nets, *Int. J. Qual. Reliab. Manag.,* **35** (2018), 2373–2387. https://doi.org/10.1108/IJQRM-06-2017-0108
10. N. Kumar, P. C. Tewari, A. Sachdeva, Performance modeling and analysis of refrigeration system of a milk processing plant using Petri nets, *Int. J. Perform. Eng.,* **15** (2019), 1751–1759. https://doi.org/10.23940/ijpe.19.07.p1.17511759

11. N. Kumar, P. C. Tewari, A. Sachdeva, Performance modelling and availability analysis of a milk pasteurising system using Petri nets formalism, *Int. J. Simul. Process Model.,* **15** (2020), 401–409. https://doi.org/10.1504/IJSPM.2020.110915
12. N. Kumar, P. C. Tewari, A. Sachdeva, Petri nets modelling and analysis of the veneer layup system of plywood manufacturing plant, *Int. J. Eng. Model.,* **33** (2020), 95–107. https://doi.org/10.31534/engmod.2020.1-2.ri.07v
13. J. A. Orlicky, *Material Requirements Planning (MRP): The New Way of Life in Production and Inventory Management,* New York: McGraw-Hill, Inc, 1974.
14. E. A. Silver, D. F. Pyke, R. Peterson, *Inventory Management and Production Planning and Scheduling,* 3 Eds., New York: Wiley, 1998.
15. R. F. Baldwin, *Plywood and Veneer-Based Products: Manufacturing Practices,* San Francisco: Miller Freeman Books, 1995.
16. A. Schramm, *Complete Guide to Hardwood Plywood and Face Veneer,* West Lafayette: Purdue University Press, 2003.
17. P. Bekhta, R. Marutzky, Reduction of glue consumption in the plywood production by using previously compressed veneer, *Holz Roh Werkst.,* **65** (2007), 87–88. https://doi.org/10.1007/s00107-006-0142-8
18. P. Bekhta, S. Hiziroglu, O. Shepelyuk, Properties of plywood manufactured from compressed veneer as building material, *Mater. Des.,* **30** (2009), 947–953. https://doi.org/10.1016/j.matdes.2008.07.001
19. I. Aydin, G. Colakoglu, Effects of surface inactivation, high-temperature drying and preservative treatment on surface roughness and colour of alder and beech wood, *Appl. Surf. Sci.,* **252** (2005), 430–440. https://doi.org/10.1016/j.apsusc.2005.01.022
20. I. Aydin, Activation of wood surfaces for glue bonds by mechanical pre-treatment and its effects on some properties of veneer surfaces and plywood panels, *Appl. Surf. Sci.,* **233** (2004), 268–274. https://doi.org/10.1016/j.apsusc.2004.03.230
21. G. I. Mantanis, R. A. Young, R. M. Rowell, Swelling of wood: Part I. Swelling in water, *Wood Sci. Technol.,* **28** (1994), 119–134. https://doi.org/10.1007/BF00192691
22. L. Blomqvist, J. Johansson, D. Sandberg, Shape stability of laminated veneer products: An experimental study of the influence on distortion of some material and process parameters, *Wood Mater. Sci. Eng.,* **8** (2013), 198–211. https://doi.org/10.1080/17480272.2013.803501
23. B. Shivamurthy, N. Naik, B. H. S. Thimappa, R. Bhat, Mechanical property evaluation of alkali-treated jute fiber reinforced bio-epoxy composite materials, *Mater. Today: Proc.,* **28** (2020), 2116–2120. https://doi.org/10.1016/j.matpr.2020.04.016
24. T. Wang, Y. Wang, R. Crocetti, M. Walinder, R. Bredesen, L. Blomqvist, Adhesively bonded joints between spruce glulam and birch plywood for structural applications: Experimental studies by using different adhesives and pressing methods, *Wood Mater. Sci. Eng.,* **18** (2023), 1141–1150. https://doi.org/10.1080/17480272.2023.2201577
25. J. F. Siau, *Transport Processes in Wood,* Berlin: Springer, 1984. https://doi.org/10.1007/978-3-642-69213-0
26. A. Pizzi, K. L. Mittal, *Handbook of Adhesive Technology,* 3 Eds., Boca Raton: CRC Press, 2017. https://doi.org/10.1201/9781315120942
27. L. Blomqvist, S. Berg, D. Sandberg, Distortion in laminated veneer products exposed to relative-humidity variations: Experimental studies and finite-element modelling, *BioResources,* **14** (2019), 3768–3779. https://doi.org/10.15376/biores.14.2.3768-3779

28. J. Friederich, S. Lazarova-Molnar, Reliability assessment of manufacturing systems: A comprehensive overview, challenges and opportunities, *J. Manuf. Syst.,* **72** (2024), 38–58. https://doi.org/10.1016/j.jmsy.2023.11.001
29. A. K. Singh, P. C. Tewari, An overview of reliability, availability, maintainability, and safety strategies for complex systems in various process industries, *Int. J. Perform. Eng.,* **19** (2023), 788–796. https://doi.org/10.23940/ijpe.23.12.p3.788796
30. A. Sheeba Angel, R. Jayaparvathy, Performance modeling of an intelligent emergency evacuation system in buildings on accidental fire occurrence, *Saf. Sci.,* **112** (2019), 196–205. https://doi.org/10.1016/j.ssci.2018.10.027
31. M. D. Smith, S. E. Schechter, *Computer Security Strength & Risk: A Quantitative Approach,* Cambridge: Harvard University, 2004.
32. S. K. Sahani, R. K. Raj, K. Sathishkumar, G. N. Keshava Murthy, S. B. Manojkumar, K. B. Naveen, et al., Mechanical Process Control and Statistical Process Control for Reducing Butter-Oil Defects in Industrial Production, *Rep. Mech. Eng.,* **7** (2026), 169–184. https://doi.org/10.31181/rme575
33. S. K. Sahani, S. K. Oruganti, K. Satish Kumar, K. Sahani, B. K. Pandey, D. Pandey, Case Study on Mechanical and Operational Behavior in Steel Production: Performance and Process Behavior in Steel Manufacturing Plant, *Rep. Mech. Eng.,* **6** (2025), 180–197. https://doi.org/10.31181/rme496